Acta Metallurgica Sinica (English Letters) (2021) 34:1173–1200
https://doi.org/10.1007/s40195-021-01249-7

A Comprehensive Overview on the Latest Progress in the Additive Manufacturing of Metal Matrix Composites: Potential, Challenges, and Feasible Solutions

Mehran Dadkhah[1] · Mohammad Hossein Mosallanejad[1,2] · Luca Iuliano[3] · Abdollah Saboori[3]

Received: 31 December 2020 / Revised: 20 March 2021 / Accepted: 14 April 2021 / Published online: 23 May 2021

Abstract
Nowadays, as an emerging technology, additive manufacturing (AM) has received numerous attentions from researchers around the world. The method comprises layer-by-layer manufacturing of products according to the 3D CAD models of the objects. Among other things, AM is capable of producing metal matrix composites (MMCs). Hence, plenty of works in the literature are dedicated to developing different types of MMCs through AM processes. Hence, this paper provides a comprehensive overview on the latest research that has been carried out on the development of the powder-based AM manufactured MMCs from a scientific and technological viewpoint, aimed at highlighting the opportunities and challenges of this innovative manufacturing process. For instance, it is documented that AM is not only able to resolve the reinforcement/matrix bonding issues usually faced with during conventional manufacturing of MMCs, but also it is capable of producing functionally graded composites and geometrically complex objects. Furthermore, it provides the opportunity for a uniform distribution of the reinforcing phase in the metallic matrix and is able to produce composites using refractory metals thanks to the local heat source employed in the method. Despite the aforementioned advantages, there are still some challenges needing more attention from the researchers. Rapid cooling nature of the process, significantly different coefficient of expansion of the matrix and reinforcement, processability, and the lack of suitable parameters and standards for the production of defect-free AM MMCs seem to be among the most important issues to deal with in future works.

Keywords Additive manufacturing · Metal matrix composite · Microstructure · Interfacial bonding · Mechanical properties

1 Introduction

Metal matrix composites (MMCs) are a class of materials that can be produced by adding one or more reinforcements to a metallic matrix [1, 2]. Over the past years, MMCs could attract worldwide attention mainly owing to their unique properties as well as the possibility to tailor the properties of materials and consequently fulfil the criteria of the particular applications [3, 4]. In fact, through the production of MMCs, it is possible to combine the ductile, tough and conductive characteristics of metals with wear resistance, stiffness, and rigidness of ceramic materials. MMCs are commonly employed as a promising class of materials to produce lightweight components and structures in different sectors such as aerospace, automotive, and construction. In particular, nowadays, a growing interest in the MMCs in both the automotive and aerospace industries confirms the worldwide demand for these materials. Nevertheless, the production of MMCs is faced with several challenges, mostly stemming from their complicated processing and incompetent economic efficiency [5].

In general, the conventional production processes of MMCs can be classified into three different groups: solid-state, semi-solid, and liquid-state processes [6]. Physical vapour deposition (PVD), diffusion bonding (DB), mechanical alloying (MA), and powder metallurgy (PM) are

Available online at http://link.springer.com/journal/40195.

✉ Abdollah Saboori
abdollah.saboori@polito.it

[1] Department of Applied Science and Technology, Politecnico di Torino, Corso Duca Degli Abruzzi 24, 10129 Torino, Italy

[2] Department of Materials Engineering, Isfahan University of Technology, 84156-83111 Isfahan, Iran

[3] Department of Management and Production Engineering, Politecnico di Torino, Corso Duca Degli Abruzzi 24, 10129 Torino, Italy

those of solid-state methods. As the semi-solid methods, compocasting and thixoforging methods have been developed to improve the distribution of reinforcement within the matrix [7]. Stirring casting, ultrasonic-assisted casting, spray deposition, and pressure infiltration methods are also developed as liquid-based manufacturing processes [8–10]. On the other hand, the production of MMCs can be divided into three main concepts from the manufacturing process standpoint: (I) casting, (II) DB, and (III) PM. Among them, PM is the only process that can be used to manufacture the MMCs reinforced by particle or whiskers that exhibit outstanding specific strength and stiffness, isotropic properties, and the ease of near-net-shape production. For this type of MMCs, various reinforcing materials such as carbides (i.e. SiC, B_4C), oxides (i.e. SiO_2, Al_2O_3), nitrides, borides, and elemental materials like C and Si, can be used [8, 11, 12].

As mentioned earlier, PM is a promising route for producing MMCs reinforced by particles. Hot pressing (HP) and spark plasma sintering (SPS) are the two main conventional manufacturing processes that have been used to consolidate the composite powder mixtures [13, 14]. However, the production of MMCs via these techniques is faced with several challenges as well. These challenges may be attributed to the interaction of matrix/reinforcement issues such as weak interfacial bonding between them and inhomogeneous distribution of reinforcement within the matrix [2]. Some of these issues become even more critical when a part with a complex geometry is required [15]. In addition, the high production cost of MMCs from the economic point of view has been considered as another important challenge that should be fulfilled to increase the application of MMCs in various industries [16, 17]. Hence, over the past years, several efforts have been undertaken to address these issues to broaden the application of MMCs. Among other things, these efforts constituted employing metal additive manufacturing (AM) techniques, a recent technology that has been rapidly developed into a promising method for the production of complex-shaped components [5, 15].

AM, which is initially developed in 1986, refers to the manufacturing process that allows the direct net shape production of 3D parts from a computer-aided design (CAD) model by progressively adding materials in a layer-wise manner [18, 19]. AM technologies provide several advantages to the production of complex-shaped parts. For instance, by using AM processes, it would be possible to eliminate the post intermediate tooling necessity, which consequently decreases the manufacturing time. Besides, AM provides opportunities to reduce materials waste, reduce energy consumption, and provide the best design for lean production [20]. Contrary to the conventional manufacturing processes, AM can produce complex geometries with a high level of design accuracy and flexibility [21, 22]. Due to the all aforementioned advantages, AM processes have been widely applied as a new manufacturing concept in various industries such as medical, aerospace, automotive [23] prototyping, and more recently in the construction industry [24, 25].

In metal AM, an energy source is employed to selectively melt a layer that solidifies afterwards. In MMCs, this energy source melts the layer and can trigger a chemical reaction if the starting powders have the potential for a chemical reaction. This selective melting/solidifying phenomenon during the metal AM process offers an exceptional flexibility to the production of complex-shaped MMCs with a homogenous dispersion of reinforcement. Therefore, several investigations have been carried out on the production of MMCs using AM technologies [26–28]. For instance, AlMangour et al. [29] produced 316L/TiB_2 stainless steel composite via laser powder bed fusion (LPBF) process. Gu et al. [30] manufactured Ti/TiC nanocomposite components using the LPBF process. In another work, Gu et al. [31] studied the feasibility of the production of AlSi10Mg/AlN via LPBF. Ramakrishnan et al. [32] fabricated functionally graded MMCs of Haynes 282/SiC via directed energy deposition (DED) process. Pouzet et al. [33] used an in situ reaction phenomenon during the DED process to produce the titanium/TiB + TiC composites from a blend of pre-alloyed Ti-6Al-4V/B_4C powder. Nonetheless, despite a growing body of literature and several reviews that have been focused on understanding the metal AM processes [34–36], the number of reviews including a comprehensive understanding of the production and performance of MMCs with metal AM processes is relatively negligible. In fact, it is well documented that the presence of reinforcements changes the physical properties of the materials and consequently affects the thermal and rheology characteristics of the melt pool [5]. As a result, MMCs would have a different processability behaviour as compared to the monolithic materials, a fact that requires further in-depth investigations. Thus, the necessity of a complete understanding of the manufacturing and performance of MMCs manufactured via metal AM processes is felt. Hence, this work aims to analyse the scientific and technological aspects of MMCs processing through AM technologies. For this reason, this review is focused on the processability of MMCs via metal AM technologies, in particular, LPBF and DED processes. At first, to provide a basic understanding of the AM approach, the AM technologies are introduced in this paper. Thereafter, the main AM methods for producing metallic components, including PBF and DED technologies, are described comparatively. This would offer a clear vision of the different technologies, including their concept together with their capabilities in the production of MMCs. An in-depth overview of the production-related aspects, including materials and AM process parameters, is then provided. Microstructure and mechanical properties of MMCs processed via AM technologies are analysed

afterwards to provide a better understanding regarding their performance. Finally, the main challenges in the fabrication of MMCs by metal AM technologies are evaluated and discussed.

2 Metal Additive Manufacturing

In general, according to the ASTM International (American Society for Testing of Materials) [37], the AM process can be classified into seven techniques, based on the adhesion and bonding method. Table 1 lists the categories, the techniques and proper materials which can be used for each process.

On the other hand, AM processes can be classified as "direct" and "indirect" processes. Direct approaches are the processes in which the shaping and consolidation of the components are performed simultaneously, and no post-processing is required to densify the parts. In fact, in these methods, the final pieces are produced by completely melting of metal powder followed by a solidification process. PBF and DED, the two main metal AM technologies, are considered as direct methods [38]. Instead, in indirect methods such as SLA, BJ, MJ, etc., since a binder is employed for the shaping, some post-processing such as debinding and sintering are necessary to consolidate the materials and consequently increase the density of components [38].

In all metal AM processes, the starting materials (metal powder or wire) are consolidated into dense 3D objects using a heat source such as laser or electron beam [39]. This work provides an overview on the development of MMCs through the metal AM processes, mainly PBF and DED technologies.

2.1 Powder Bed Fusion (PBF)

In all PBF processes, a layer of powder is spread on the building platform or previously solidified layers, which is consequently melted in a selective manner according to the CAD model. The spread of a layer of powder followed by selective melting via local heating is repeated until the entire part is printed. The focused source of energy used for the PBF technique can be either electron beam or laser beam that classifies the techniques into two categories of laser powder bed fusion (LPBF), also known as selective laser melting (SLM) and electron beam melting (EBM) [40]. The number of publications regarding PBF acquired from the Scopus database is shown in Fig. 1. It is shown that since 2000, there is a growing body of literature published on the LPBF and EBM methods. According to the Scopus database, the overall number of publications on these two technologies has exponentially increased to several thousands of papers (almost more than 11,000) by 2020. However, it is found that despite the growth of these technologies (Table 2), the development of new materials specifically developed for AM requires more attention which justifies carrying out more

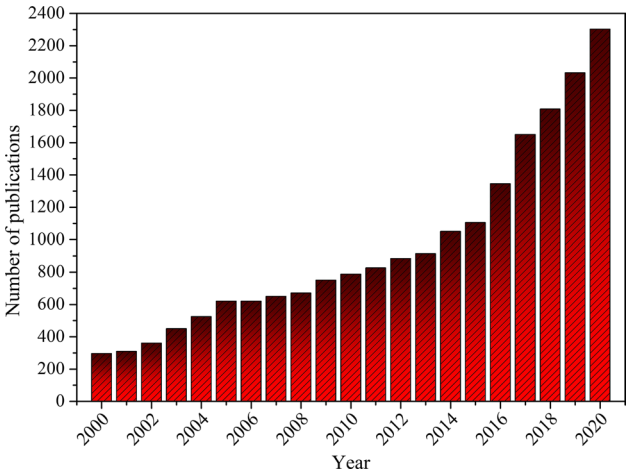

Fig. 1 Number of publications on SLM and EBM as keywords (Scopus, 30 December 2020)

Table 1 ASTM International classification of AM [37]

Category	VAT	BJ	MJ	SL	ME	PBF	DED
Process	SLA DLP	3D printing Ink-jetting S-Print M-Print	Polyject Ink-jetting Thermojet	UC LOM	FDM	SLS SLM EBM	DMD LD LC EBDM
Materials	Photopolymer Ceramic	Metal Ceramic Polymer	Photopolymer Wax	Metal Ceramic Hybride	Photopolymer Wax	Metal Ceramic Polymer	Metal (powder, wire)

SLA stereolithography, *DLP* digital light processing, *UC* ultrasonic consolidation, *LOM* laminated object manufacturing, *SLS* selective laser sintering, *SLM* selective laser melting, *EBM* electron beam melting, *DMD* direct metal deposition, *LD* laser deposition, *LC* laser cladding, *EBDM* electron beam direct melting, *FDM* fused deposition modelling

researches focused on the development of new alloys and new MMCs to be processed via PBF techniques.

However, it should be noted that even if there is a closely similar concept behind EBM and LPBF processes, the processing steps are quite different. Therefore, these differences are highlighted in this work and compared with the DED process, which is a wire/powder-fed AM technology.

2.2 Laser Powder Bed Fusion

As mentioned earlier, LPBF is one of the direct AM processes where the powder particles are fully melted during the process resulting in much stronger final 3D components with approximately 100% density [41, 42]. In this method, as shown in Fig. 2, a thin layer of metal powder is spread across the metal build plate through a delivery system of powder. Thereafter, the cross-section of metal powder is selectively scanned by a high-energy laser beam leading into melting and consolidating of powder particles into a homogenous and dense part. Extra materials that are not part of the 3D model play as a support structure and remain unaffected. Afterwards, the build platform moves down as much as a pre-defined layer thickness, followed by the coating process aimed at creating the next layer. Subsequently, the laser scanning of the next layer is carried out, and the process continues until the final 3D component is completely produced [43–45]. After the part is completely formed, extra powders are directly collected from the build chamber and recycled [46].

In comparison with conventional manufacturing processes, LPBF presents some advantages such as the ability to produce complex parts, the capability to increase the functionality of the new structural products, the capability to join various metals via metallurgical means and rapid prototyping. These benefits led to the extensive use of LPBF in industrial applications such as aerospace, automotive, electronics, and biomedical devices [47]. For instance, Song et al. [48] analysed the production of the metal die with a low cost and short process cycle to be used as an automobile deck part. In the research carried out by Wits et al. [49], high-pressure and low-weight micropumps were produced to be used in small satellite applications. Hou et al. [50], Wong et al. [51], and Zenou et al. [52] explored the application of the LPBF process in the production of electronic devices such as circuit boards, heat sinks, and transparent conductors. Besides, the LPBF process has been employed in medical applications for producing customized bioimplants [53–55]. Recently, new materials, including metal matrix nanocomposites (MMNCs) [56–58] and functionally graded materials (FGMs) [59–61], are developed through the LPBF technology.

Nevertheless, LPBF suffers from some disadvantages such as intense interaction between material and laser, the

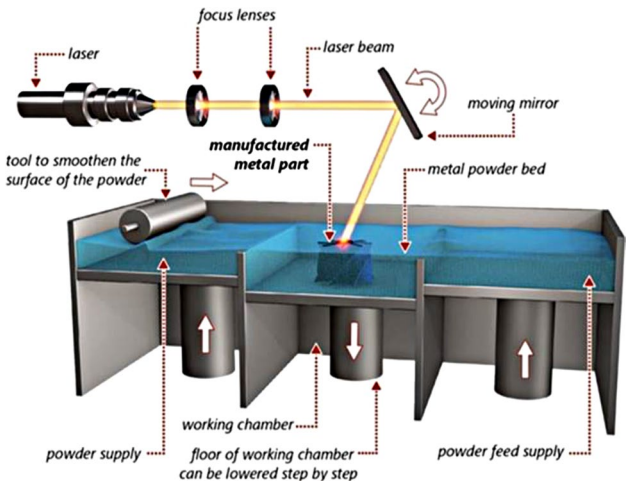

Fig. 2 A schematic of a LPBF system [41]

Table 2 Some commercially available PBF systems for metallic materials

Manufacturer	System	Process	Layer thickness (μm)	Laser spot size (μm)	Energy source
Prima additive	PrintSharp 250	LPBF	20–100	70–100	Yb-fibre laser, 500 W
SLM solutions	SLM500	LPBF	20–74	80–115	Quad fibre lasers, 4×700 W
EOS	M400	LPBF	N/A	90	Yb-fibre laser, 1000 W
Concept Laser	M1Cusing	LPBF	20–80	50	Fibre laser, 200–400 W
Realizer	SLM300i	LPBF	20–100	N/A	Fibre laser, 400–1000 W
Farsoon	FS271	LPBF	20–80	40–100	Yb-fibre laser, 200 W
Renishaw	AM400	LPBF	N/A	N/A	Optical fibre, 400 W
Sisma	MYSINT300	LPBF	20–50	100–500	Fibre laser, 500 W
Arcam AB	Q20 plus	EBM	140	–	Electron beam, 3000 W
Arcam AB	A2X	EBM	50–100	–	Electron beam, 3000 W
Arcam AB	Spectra H	EBM	N/A	–	Electron beam, 6000 W

high degree of shrinkage, instability of molten pool, and complex residual stress [62].

2.3 Electron Beam Melting

As mentioned earlier, EBM is one of the PBF processes where an electron beam is applied for the full melting of powder particles. In 1992, the first patent [63] was recorded to describe the fusion of conductive powders using an electric beam to fabricate a 3D part in a layer-wise manner. However, the first commercial EBM system was not presented until 2002 [64], which belonged to the Arcam company. It should be noted that, due to the utilization of an electron beam, this process should be carried out under a vacuum environment because of the improvement of the electron beam quality, prohibition of the electron beam dissipation and prevention of powder contamination or the fabricated components [65, 66]. In this technology, at a high temperature, the electrons are emitted from a filament, and two magnetic fields control the electron beam with the rate of half of the light speed. One of the fields works as a magnetic lens focusing the beam to the proper diameter, while the focused beam is deflected by another field to melt the desired points. In this process, a layer of powder is spread on the build platform, followed by preheating and melting of powders carried out by electron beam according to the digital data (as shown in Fig. 3). The build platform is lowered, and the next layer of powder is spread, followed by preheating and then melted ageing according to the CAD model. Finally, the 3D components are built by repeating these steps [65].

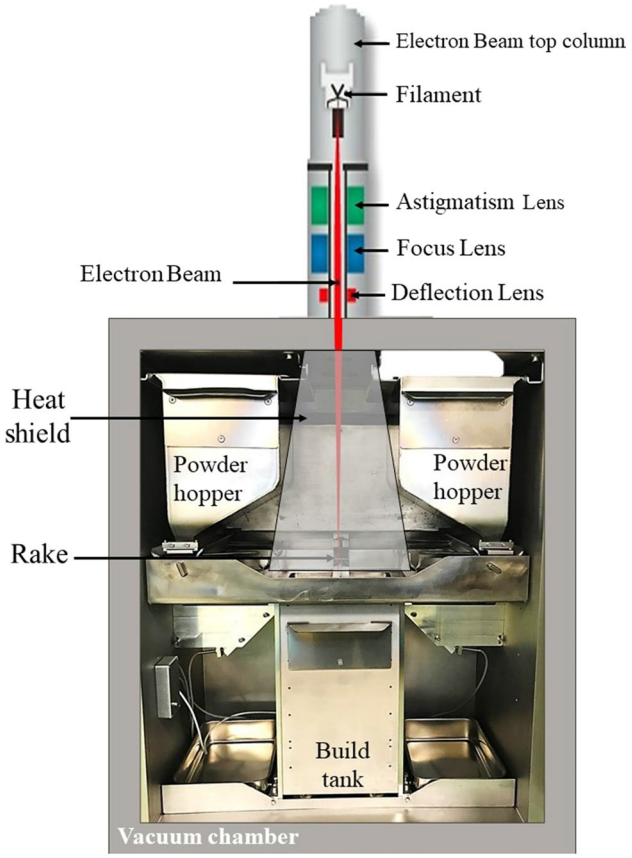

Fig. 3 A schematic of electron beam melting (EBM)

After producing the final part, as same as the other AM processes, the additional powder should be eliminated from the build chamber. In the EBM technique, these powders pass through a powder recovery system (PRS) in order to eliminate and recover the sintered powders around the parts [46]. EBM process is featured with a higher energy density than the LPBF technique, enabling this AM method to have powder layers with higher thicknesses (higher than 50 µm). Considering this, the particle size distribution of the starting powder can be in the range of 45–150 µm (larger than LPBF, which is in the range of 15–50 µm). Nevertheless, some drawbacks occur at high production rates, such as finishing and inferior surfaces [38]. As reported in the literature [67, 68], the resolution and surface roughness of EBM components are lower and higher than LPBF, respectively. Studies have compared the powder recyclability in EBM and LPBF and found that they are rather similar [69–71]. In contrast to LPBF, a vacuum atmosphere (around 1×10^{-5} mbar) is applied in the EBM chamber, which is useful to avoid any contamination, especially for the processing of reactive materials such as titanium alloys or gamma titanium aluminide intermetallics [72]. Moreover, since EBM employs a different source of energies, compared to the one used in LPBF, higher scanning rates and generally preheating of the powder (even up to 1100 °C) is possible. As a matter of fact, the powders' preheating before melting reduces the thermal stress generated during the building process [73]. The lower level of residual stress decreases the risk of crack formation and hence enables the production of rather brittle materials such as intermetallics [74–77].

In general, EBM technology is capable of producing extremely complex parts, making it suitable for the manufacturing of materials with special features [64] such as bulk metallic glass [78, 79], Ti-6Al-4V lattice structures [80], and 316L stainless steel [81, 82]. An additional advantage of this technology is the possibility to tailor the microstructure and consequently, the properties within the components in the same process through the adjustment of the process parameters [83–85].

2.4 Directed Energy Deposition

DED technology is a powder/wire feed process in which the powder/wire is delivered into the molten pool that is generated by a heat source. In fact, in DED, feeding of starting materials is simultaneously carried out with irradiation of a concentrated energy source (such as electrons beam, plasma arc or laser) on a certain area of the substrate, whereas in the PBF method, an already distributed powder bed is selectively fused [86]. At the same time, feedstock (Fig. 4 a, b) is continuously fed via either a single nozzle or multi-nozzles into the melt pool. Various processes are named DED technology, as listed in Table 3 [34, 87]. It should be highlighted that fully dense components with highly controllable microstructure properties and FGM components can be fabricated using the DED process [88].

Poor resolution, low power efficiency, and lower surface quality can be considered as the main disadvantages of this process [91]. Table 4 summarizes the difference between the DED and PBF processes from various aspects. In contrast to the LPBF process, no powder bed is applied in the DED method and also the starting materials are fused and deposited in a layer-wise manner which can be useful to fill the cracks and to retrofit the manufactured parts. Furthermore, DED is able to manufacture components with less complexity as compared with PBF methods. That's why DED is generally utilized in the manufacturing and repairing of larger parts [88]. This is very interesting to note that due to the presence of a carrier gas that delivers the feedstock material directly into the melt pool, application of the DED process in the production of MMCs could attract more attention. In most cases, when the powder mixture has poor flowability due to the presence of irregular shape reinforcements, the carrier gas facilitates the powder feeding.

Table 3 Different commercialized names of DED process [34, 90]

Process	Acronym
Laser cladding	LC
Laser direct casting	LDC
Laser engineer net shaping	LENS™
Direct metal deposition	DMD
Direct light fabrication	DLF
Shape deposition manufacturing	SDM
Laser powder fusion	LPF
Laser-aided direct metal deposition	LADMD
Laser-aided manufacturing process	LAMP

3 Additive Manufacturing of MMCs

In general, the production of metallic components via conventional manufacturing methods is costly and time-consuming. In addition, in MMCs, the presence of hard reinforcing materials can make their fabrication processes even more challenging and expansive. For this reason, several efforts have been undertaken to develop new and highly flexible techniques for the production and design of net-shape MMC components. AM produces not only net shape MMCs components but also is capable of imparting mechanical characteristics comparable to or even higher than those brought by the conventional manufacturing processes. The advantages of AM in comparison with the conventional manufacturing processes could bring attention from various industrial sectors to this technology, which has been labelled as the "Third Industrial Revolution".

Over the last decade, several research studies focused on AM of metallic materials for different industrial sectors [72, 98–100]. On the contrary, far too little attention

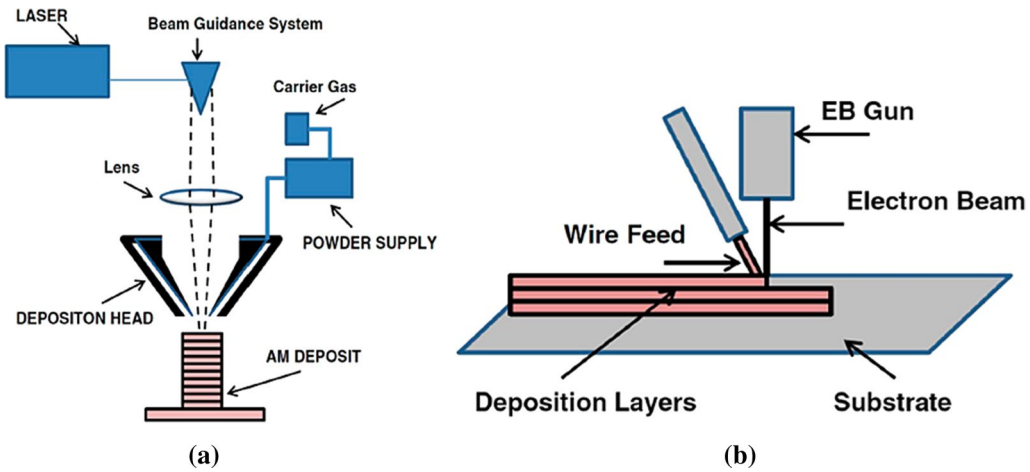

Fig. 4 Schematic of **a** powder-fed, **b** wire-fed DED process [89]

Table 4 Comparison of DED and PBF processes [90, 92–97]

Differences	SLM Process	EBM Process	DED Process
Heat source	Laser	Electron beam	Laser/Electron beam/Electric arc
Source of power (W)	200–1000	3000	100–3000
Size of beam (mm)	0.1–0.5	0.2–1.0	2–4
Environment of build chamber	Ar/N_2	Vacuum/He bleed	–
Max dimension of component (mm×mm×mm)	500×350×300	350×380 ($\phi \times H$)	(2000×1500×750) (5000×3000×1000)
Build envelop	Limited	Limited	Large, Flexible
Build ability	Complex geometry, very high resolution	Complex geometry, good resolution	Relatively simpler geometry, less resolution
Layer thickness (μm)	20–100	50–200	500–1000
Maximum rate of feedstock (g/s)	–	–	0.1–2.8
Maximum rate of production (cm^3h^{-1})	20–35	80	16–320
Maximum feature size (μm)	40–200	100	40–200
Dimensional precision of (mm)	0.04–0.2	0.04–0.2	0.5–1.5
Surface finishing	Very good	Good	Coarse
Geometric tolerance	±0.05–0.1	±0.2	–
Residual stress	High	Minimal	High
Addition of metal on existing parts	Not possible	Not possible	Possible
Build of multi-material/Hard coating	Not possible	Not possible	Possible
Post-processing	Stress relieve, HIP (rarely)	HIP (rarely)	Stress relieve, HIP, Machining, Surface grinding
Resolution range (μm)	80–250	80–250	250
Preheating process of powder	Platform heating	Preheat scanning	Platform heating
Preheating temperature of powder (°C)	100–200	700–1100	–
Size of melting pool (mm)	0.1–0.5	0.2–1.2	–
Advantages	Fine resolution High quality		Reduced cost of manufacturing Great mechanical properties Precise control of microstructure and composition Excellent for repairing and retrofitting
Disadvantages	Slow printing Expensive manufacturing		Low accuracy and quality of surface Restriction in manufacturing of complex parts including fine details
Applications	Biomedical, Electronics, Aerospace, Electro-packaging		Aerospace, Automotive, Die repair

has been paid to the AM of MMCs. This discrepancy in the trend of monolithic alloys and MMCs can be related to two major challenges in the production of MMCs via AM processes. The first challenge is related to the initial feedstock, i.e. powders of MMCs. In general, it is well documented that one of the main criteria for the AM powders is the necessity of having spherical morphology. For this reason, gas-atomized or plasma atomized powders are considered as the most desirable powders for AM. However, the composition of atomized powder for AM of monolithic alloys is rather limited, and there is no feedstock in the case of composites. On the other hand, metallic matrixes and reinforcing materials may have markedly different melting points that make some challenges for the processability of those powder mixture via AM. This difficulty can be ascribed to their different viscosity and melting/solidification behaviours. Therefore, in the case of MMCs, optimization of process parameters should be carried out carefully to fabricate MMCs components with high relative densities. However, despite several efforts that have been undertaken to address these challenges, there is no overview on the dependency of challenges on the type of reinforcing material and metallic matrixes. Therefore, this work provides a systematic and comprehensive overview on the recent progress in the AM of some very well-known MMCs such as aluminium and titanium, considering the challenges in their fabrication via AM and structure–property relationship in these composites.

3.1 Feedstock Preparation

To fabricate a MMC through AM processes, the starting point is the preparation of the composite powder mixture. In general, an ideal powder mixture should exhibit a uniform elemental distribution as well as good flowability. Up to now, several methods such as ball milling, powder electrostatic self-assembly, and in situ reaction have been proposed for the preparation of the composite powder mixtures. In ball milling, to increase the bonding between the matrix and reinforcement, hard grinding balls are placed in the milling media together with the powder mixture. During the milling process, the forces between the balls create bonds between the matrix and reinforcement particles. These forces, however, can deform the particles and consequently reduce the flowability of the powder mixture significantly. Accordingly, this lower flowability would negatively affect the processability of the composite powder mixture [101]. Therefore, to resolve this issue which is related to the deformation of particles, the electrostatic self-assembly method has been developed. In this method, an electrostatic attraction is created by inducing a positive and negative charge to the particles, leading to a uniform powder mixture [102]. Nevertheless, this method suffers from challenges such as a complex preparation process and low efficiency, limiting its application for composite powder preparation. As an alternative, the in situ reaction method is proposed to be used as a more efficient method to prepare a composite powder mixture through the addition of the reinforcing material in the molten state, and after a while, the molten material is atomized into powders [103]. In comparison with the other two mixing methods, the in situ reaction process is considered as an ideal method in terms of making a uniform powder mixture with an acceptable morphology and good flowability. However, this method has some disadvantages; among them, the complexity and cost of the process can be considered as the main ones. Moreover, in situ reactions leading to the desired secondary phases are not appropriate for all the composite systems, and hence, it can only be applied for some certain cases.

3.2 Processability

3.2.1 Aluminium Matrix Composites (AMCs)

AMCs are considered as a new substitute for Al alloys due to their excellent specific stiffness, wear resistance and outstanding structural integrity and physical properties [104, 105]. From the industrial point of view, AMCs can be produced through two main class of manufacturing processes: (I) solid-state and (II) liquid-state processes. Diffusion bonding and vapour deposition processes are two important solid-state-based production processes of AMCs, whereas casting, infiltration, and in situ processing are the liquid-based ones [106]. It is well documented that the real applications of AMCs, in addition to the properties of the material, strongly depend on their ease of production. In general, casting, which is considered as one of the most promising methods for the production of Al alloys, suffers from undesired reactions and also a serious lack of control on the dispersion of the reinforcing material within the matrix in the case of AMCs. Moreover, further machining of the cast components reinforced by hard reinforcements is a very difficult task, which increases their production cost significantly.

PM methods such as metal AM processes can overcome these challenges via point-by-point material consolidation. Therefore, it can be expected that through the combination of metal AM advantages (in particular laser-based ones), such as high processing precision, short production cycle, and customized production feasibility, with the aforementioned characteristics of the AMCs, fully dense near-net-shape AMCs with superior properties can be produced. Since AM is a rapid solidification process, the microstructure of as-built AM AMCs is finer than those of conventional one, which further strengthens the final AMCs product.

During the production of Al alloys via an AM process, the Al powder is melted locally through the irradiation of the laser, which then creates a melt pool quickly solidifying via nucleation and directional growth mechanisms. Typically, in the case of monolithic Al alloys, the columnar microstructure is observed due to the absence of heterogeneous nucleation sites and the presence of a very high thermal gradient along the building direction [107, 108]. During the interaction of the laser with the Al powder, the Marangoni convection is a fluid flow mechanism taking place in the melt pool that helps the reinforcing materials to be distributed homogeneously in the liquid. On the other hand, as mentioned earlier, since the molten material is solidified in the metal AM processes rapidly, there is not enough time for a detrimental reaction between the Al matrix and reinforcement phase. Therefore, this rapid solidification process results in the formation of very fine second phases that, together with the unreacted reinforcement, create multi-phase reinforced AMCs [109, 110]. As a result of this coexistence of reinforcement and the fine second phase, the microstructure of AMCs turns from the columnar to equiaxed or to the columnar with a small aspect ratio (Fig. 5) [111].

It is also very interesting to notice that due to a significant difference in the melting point of the Al matrix (about 660 °C) and reinforcing materials (typically more than 2000 °C), these reinforcements can significantly improve the laser absorption of the Al alloy and increase the efficiency of the processes [109].

Laser energy density, which defines the amount of heat input during the laser interaction with the alloy, is found to be another important factor having a marked effect on the

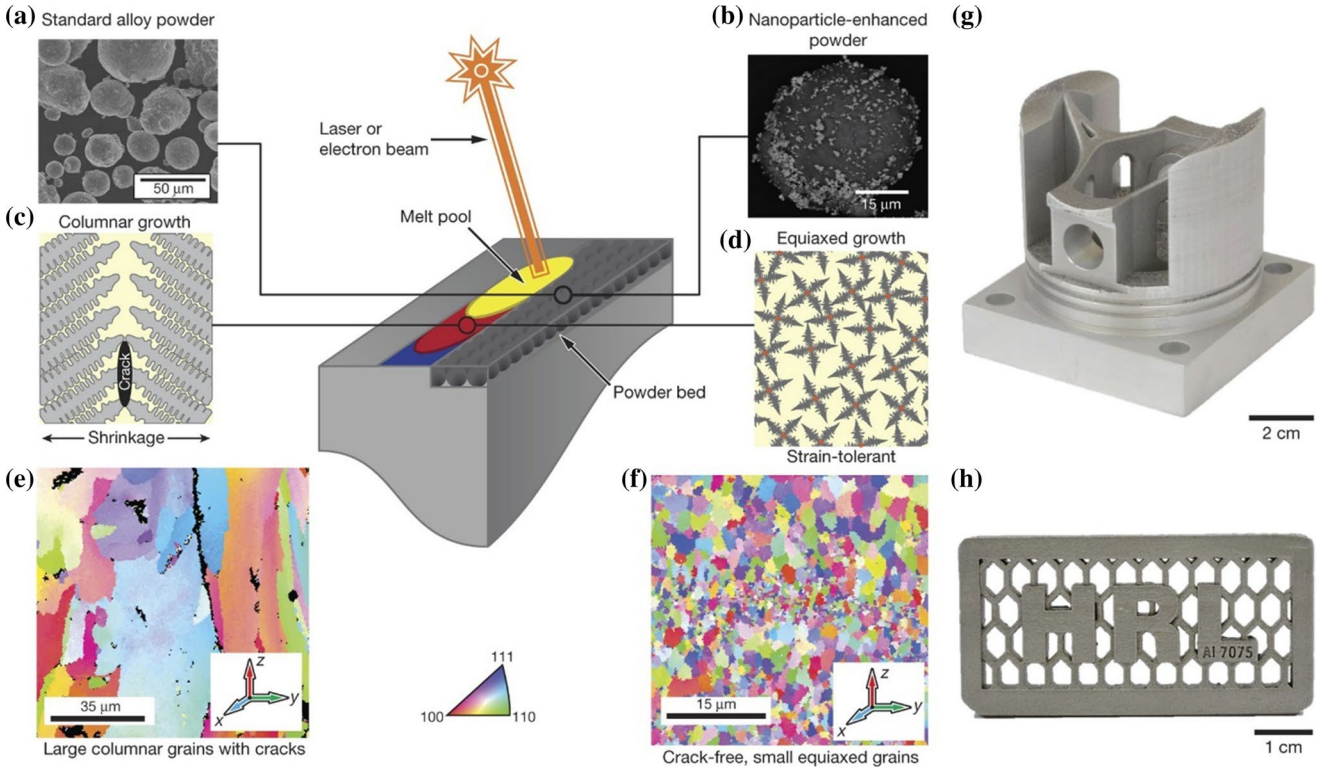

Fig. 5 Central schematic represents an overview of the AM: **a** unreinforced Al7075 powder, **b** reinforced Al7075 powder, **c** Al7075 tend to solidify by columnar growth of dendrites, **d** suitable nanoparticles can induce heterogeneous nucleation and facilitate equiaxed grain growth, **e** many alloys exhibit intolerable microstructure with large grains and periodic cracks when AM using conventional approaches, as illustrated by the inverse pole figure, **f** functionalizing the powder feedstock with nanoparticles produces fine equiaxed grain growth and eliminates hot cracking [102]

microstructure of AMCs. For instance, Lei et al. [112] studied the impact of the energy density on the microstructure formation and microhardness of the LPBF 7075 Al alloy modified by Sc and Zr. They found that at low energy density, the grains grew epitaxially, and as a result, columnar grains with an average size of 4.1 µm were formed. However, they reported columnar to equiaxed transformation by increasing the energy density, which increased the number of equiaxed grains with an average size of 0.78 µm (Fig. 6).

In another work, Gu et al. [111] studied the microstructure and mechanical properties of AlSi10Mg/CNTs composites produced via the LPBF process. They found that by increasing the laser scanning speed, the microstructure of the AMC reinforced by CNTs transformed from the coarse columnar crystals to the equiaxed ones. Jue et al. [113] investigated the mechanical properties and microstructure of in situ Al/Al_2SiO_4 composites produced via LPBF. According to the authors' findings, by decreasing the energy density, the grain size of AMCs decreased first and then increased. This trend was explained by the correlation between the energy density and the maximum temperature gradient of the melt pool that promoted the reinforcement and Al matrix reaction. In fact, the degree of in situ reaction increased by increasing the energy density, and as a consequence, more nucleation sites for the heterogeneous nucleation were formed, leading to the grain refinement. However, at very high energy densities, since the melt pool remained liquid for a bit longer time at high temperatures, the reaction between the reinforcement and Al matrix was completed. Therefore, the number of nucleation sites decreased significantly, leading to grain coarsening. Among all the ceramic reinforcements, TiB_2 is one of the most interesting materials to be used as a reinforcing phase for developing new AMCs. TiB_2 does not react with the Al matrix and significantly participates in the strengthening of the composite [114].

Jiang et al. [101] analysed the microstructure and mechanical performance of 7075Al/TiB_2 composites produced via the DED process. Despite a non-uniform dispersion of TiB_2 within the Al matrix, slight grain refinement was achieved in the samples containing 4 wt% TiB_2. Wen et al. [115] also reported the same trend in their studies on 2024Al/TiB_2 composites produced via DED. In another study, Li et al. [103] evaluated the effect of nano-TiB_2 on the microstructural evolution of the AlSi10Mg alloy produced via the LPBF process. As shown in Fig. 7, they obtained a texture-free microstructure consisting of fine

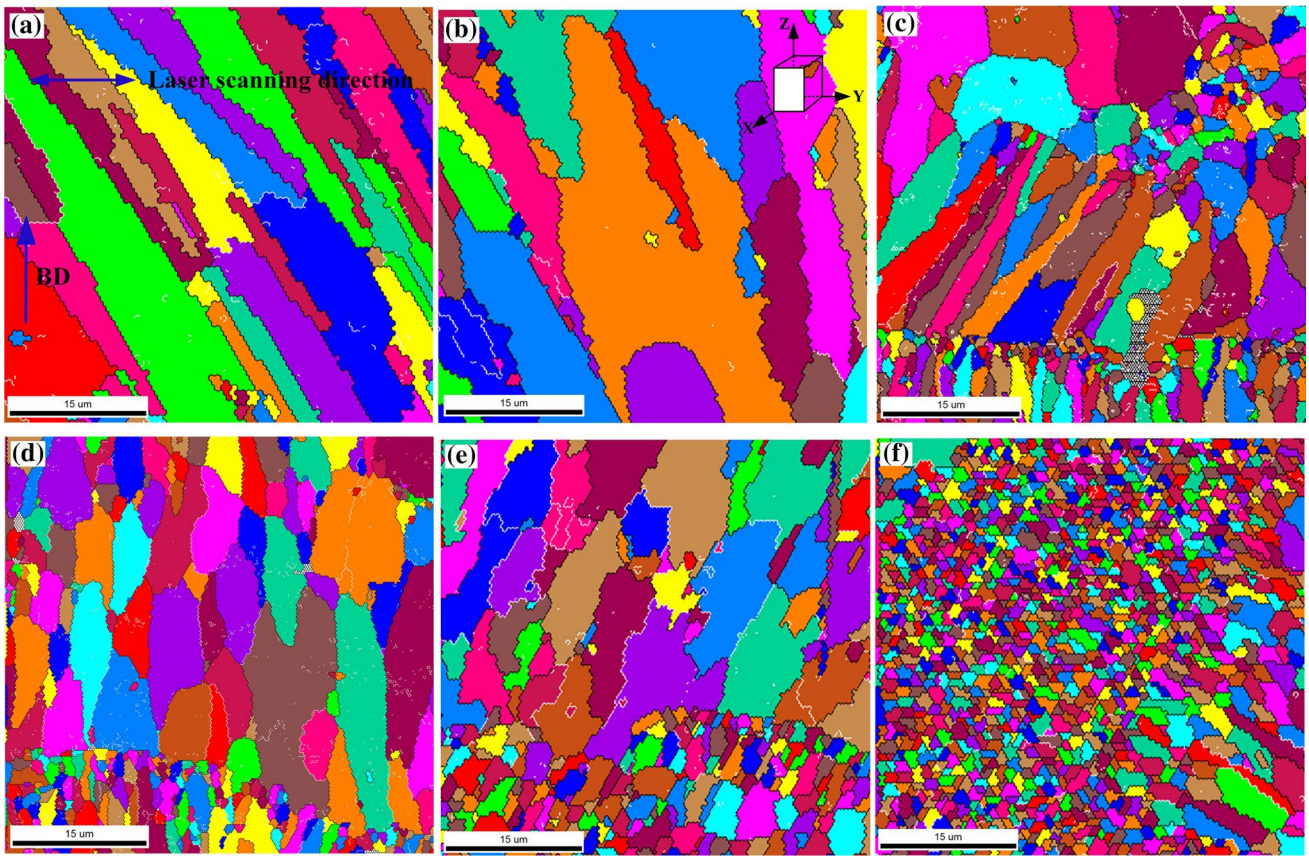

Fig. 6 EBSD images of block specimen at different energy densities: **a** 44 J/mm^3, **b** 66 J/mm^3, **c** 111 J/mm^3, **d** 222 J/mm^3, **e** 333 J/mm^3, and **f** 375 J/mm^3 [112]

grains and a cell structure. It was also revealed that the nano-TiB_2 particles have a preferred distribution being mainly located along the cell boundaries with some nano-TiB_2 agglomerates seen in the triple pockets of the cells. As mentioned earlier, in the case of AMCs, the coexistence of the fine grains and reinforcement results in superior mechanical and physical characteristics compared to the monolithic Al alloys. In nano-AMCs, i.e. AMCs reinforced by nanomaterials, the presence of nanoscale reinforcements results in the formation of ultrafine grains. Wen et al. [115] used nano-TiB_2 particles to strengthen 2024Al alloy produced via the DED process. In their 2024Al-3 wt% TiB_2 nanocomposites, the high tensile strength of 284 MPa and excellent ductility of 18.7% were achieved, which were much higher than those of 2024Al alloys produced by casting. Li et al. [103] studied the microstructure and mechanical properties of LPBF AlSi10Mg nanocomposite reinforced by 7 vol% nano-TiB_2 particles. The results showed that nano-AMCs had a high tensile strength of 530 MPa, excellent ductility of 15.5% and microhardness of 191 HV, marking the best mechanical properties ever published for the AMCs based on AlSi10Mg alloy.

Graphene (Gr) and carbon nanotubes (CNTs) are rather new reinforcing materials for AMCs. In fact, these carbonic materials react with molten Al during the AM process and form aluminium carbide (Al_4C_3) with different morphologies. These carbon-bearing products play a key role in the strengthening of the AMCs. During the irradiation of the laser, the input energy is first absorbed by graphene or CNTs that results in the partial decomposition of Gr or CNT, followed by their in situ reaction with the Al matrix and consequently the formation of Al_4C_3 at their interfaces [111]. In addition, when an AMC reinforced with CNTs is subjected to external forces, the oriented CNTs in the loading direction play a key role in the strengthening of the composite [104, 116]. Zhou et al. [117] used graphene oxide as a reinforcement for AMC production through the LPBF process. In their work, Al_4C_3 nanorods were reported as the products of the reaction between the reinforcement and pure Al matrix. Ma et al. [118] reported the formation of nanoplate Al_4C_3 near the interface of the diamond/AlSi12 composite produced via LPBF technology (Fig. 8).

More recently, Tiwari et al. [119] assessed the effect of 0.1 and 0.2 wt% Gr on the microstructure and mechanical

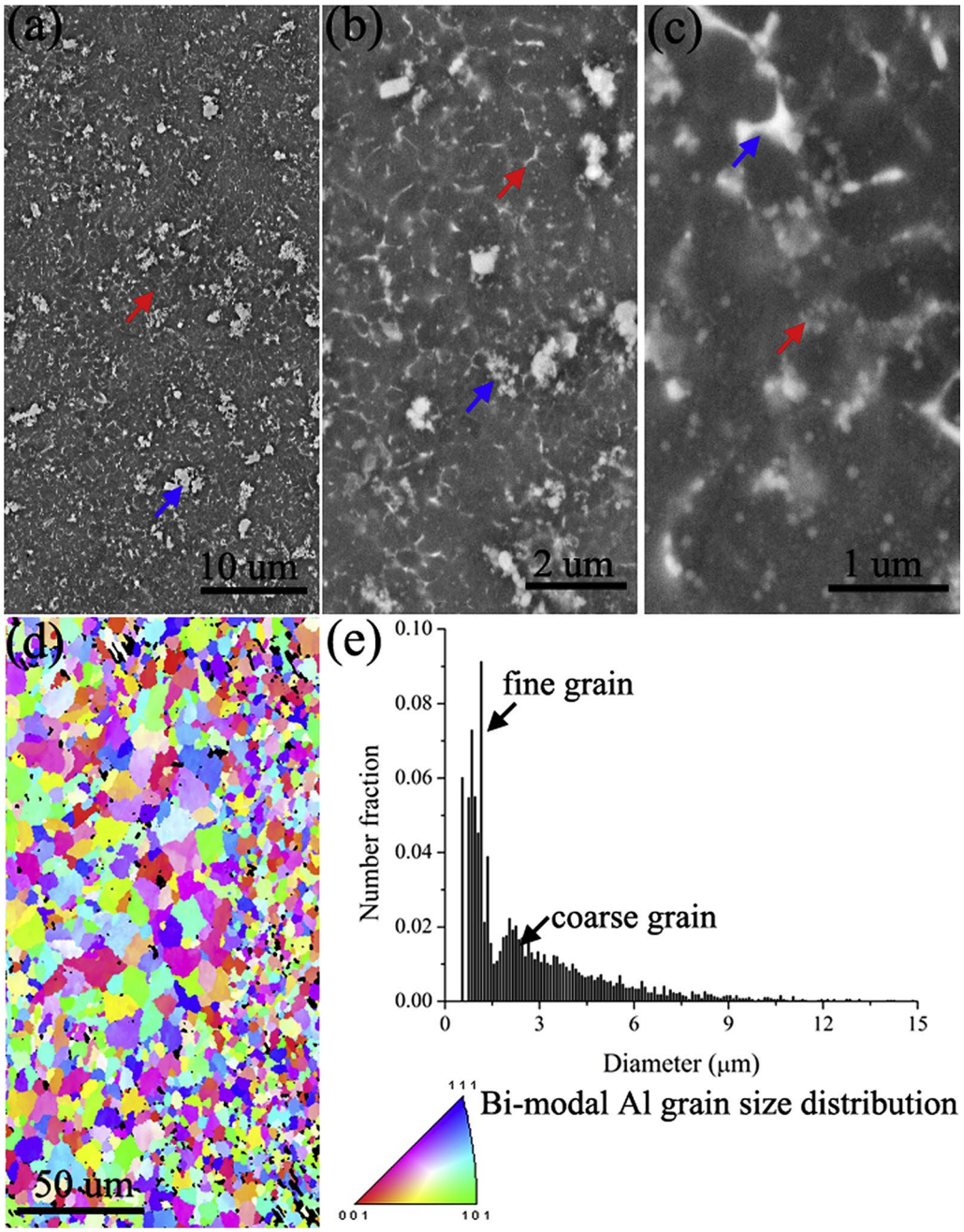

Fig. 7 **a**–**c** SEM images, **d** EBSD orientation map, **e** grain size distribution of the LPBF Al composites [103]

characteristics of the AlSi10Mg-based composites fabricated using the LPBF method. They reported tensile properties of samples as being remarkably influenced by the induced porosity after incorporation of Gr. The authors reported an approximate of 22% increment in yield strength (YS) of the samples in the presence of 0.1 wt% Gr, in contrast to the elongation of the composite showing a decreasing trend (Fig. 9). According to Fig. 10, incorporation of 0.2 wt% Gr had a significant effect on the hardness of the samples, while the laser power variation had no effect on the hardness.

Gu et al. [111], studied the effect of CNTs on the microstructure evolution and mechanical properties of AlSi10Mg composites produced via the LPBF process. From the microstructural point of view, three distinct phenomena, namely the formation of the primary Al9Si cellular dendrites decorated with fibrous Si, the in situ formation of Al_4C_3 on the CNTs, and precipitation of Si inside the cellular grains, were revealed. AlSi10Mg/CNTs composites featured superior mechanical properties (tabulated in Table 5) due to the microstructure being ultrafine and having a high

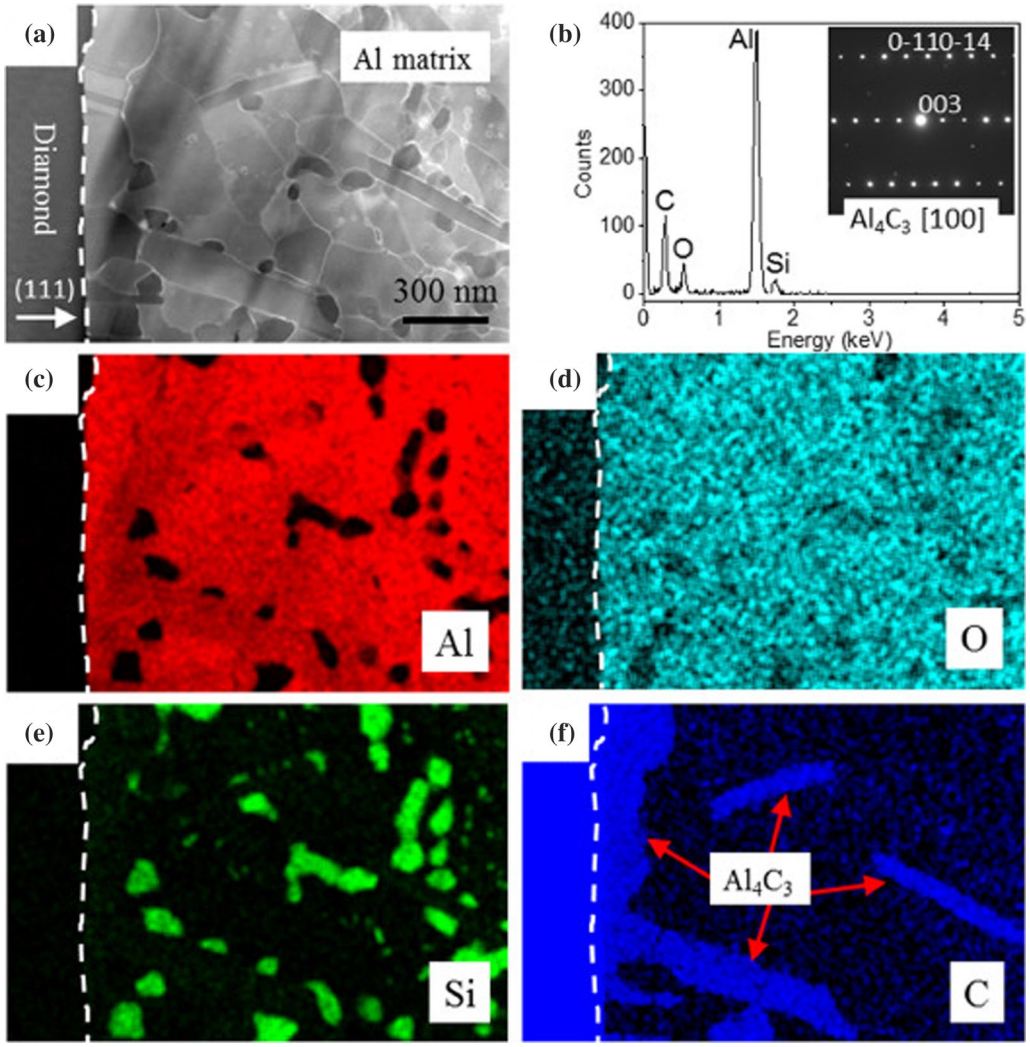

Fig. 8 **a** Scanning TEM (STEM) high-angle annular dark-field (HAADF) image showing the diamond(111)/Al interfacial area where Al_4C_3 interfacial layer and plate-like particles are developed, **b** the EDX spectrum of a typical interfacial particle is shown, **c**–**f** are elemental EDX maps for Al, O, Si, and C, respectively [118]

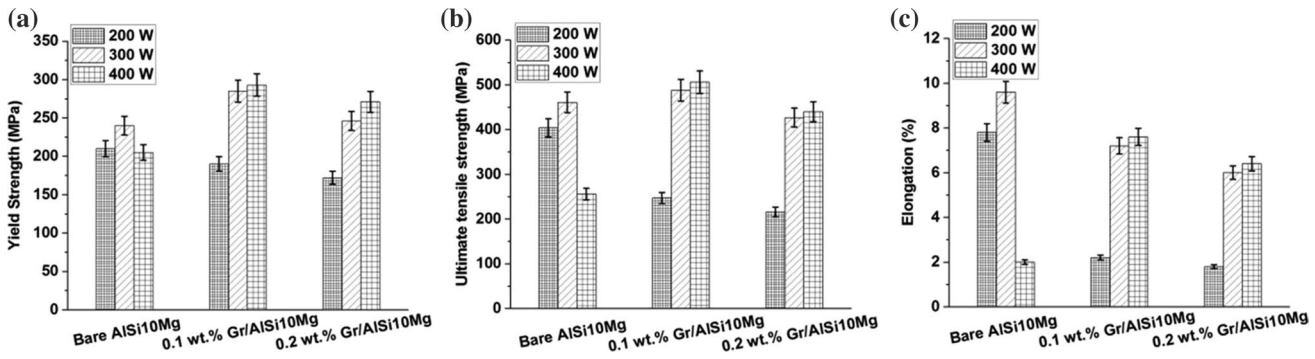

Fig. 9 Tensile properties of the pure AlSi10Mg, AlSi10Mg-Gr composites at different laser powers; **a** YS, **b** UTS, and **c** Elongation [119]

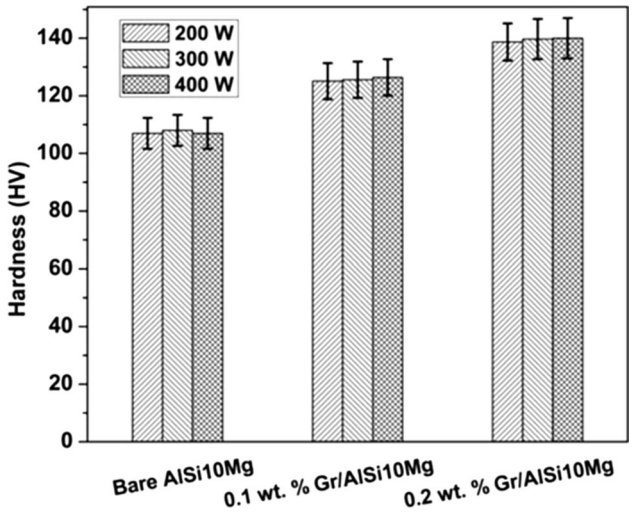

Fig. 10 The hardness of the pure AlSi10Mg, AlSi10Mg-Gr composites at different laser powers [119]

densification level. Nonetheless, it should be highlighted that the structure of Gr can be damaged during the interaction with laser marking a weak point to the mechanical performance of the composite. Notwithstanding, it is reported that the presence of these types of reinforcements improved the hardness and tribological characteristics of the AMCs [120]. As an example, Bai et al. [121] analysed the effect of Gr on the microstructure and wear resistance of AMCs produced by the LPBF process. They found that at low Gr contents, the wear resistance of the composite increased while it followed a decreasing pattern by increasing the Gr content as a consequence of the Gr agglomeration and formation of higher porosity within the AMCs. Instead, Jiang et al. [101] exhibited that the addition of TiB_2 particles as reinforcement improves the wear resistance of the 7075Al-based composite produced by the DED process.

All in all, it can be concluded that AMCs reinforced by nanoparticles exhibit superior comprehensive mechanical properties with respect to those using micron size reinforcements. However, AMCs reinforced by microparticles present higher hardness and wear resistance in comparison with Al alloys. In these systems, the microparticles act as stress concentration sites and hence their effect on the mechanical properties is not stable. On the other hand, in the case of using nanoparticles, their ease of agglomeration deteriorates the flowability of the powder, which reduces the processability of the AMCs powder mixture. Moreover, using carbonaceous reinforcements like CNTs and Gr results in outstanding tensile and compressive properties, increasing in hardness and wear resistance of the AMCs.

Finally, it is worth mentioning that despite of all the R&D efforts that have been made on the production of AMCs via AM process, still there are some challenges and barriers that limit their production. These challenges can be listed as follows: (I) Agglomeration of the reinforcing material at their higher contents reduces the flowability and, consequently, the powder's processability. (II) For AM AMCs, the wear properties for the microreinforced composites are better, whereas the mechanical performance and plasticity are higher in nano-reinforced ones. Therefore, further researches on AMCs are necessary to evaluate the effect of reinforcement size and content on each property of AMCs. (III) Using carbonaceous reinforcements needs extra analysis to evaluate their structure after the laser irradiation. In fact, if their structures are damaged significantly, it can deteriorate the mechanical properties significantly. (IV) AM can be used only with discontinuous reinforcements.

3.2.2 Titanium Matrix Composites (TMCs)

Ti-based alloys are considered as promising materials for various industries, including biomedical, automotive, chemical engineering, marine, and aerospace. This wide range of applications for the Ti-based alloys is attributed to their outstanding combination of high specific strength that remains up to the high temperatures, excellent mechanical characteristics, excellent biocompatibility, and outstanding corrosion resistance [72, 130–132]. However, these alloys can potentially be considered for greater applications if their properties can be enhanced even more than those exhibited by the Ti alloys produced via conventional technologies. In fact, under the circumstances Ti alloys are given competitive performance and cost by tailoring the processing method, they can potentially substitute other metallic materials. Therefore, this great motivation resulted in the development of the new Ti matrix composites with superior features and performances [133].

Casting, forging, and PM are the conventional manufacturing processes that have been used to produce the Ti-based parts so far [134]. In the production of Ti components, conventionally, there is a post-processing step such as surface finishing, machining, and heat treatment aimed at improving the performance and final properties of the components for the final applications. However, low thermal conductivity as well as high reactivity of Ti create lots of challenges for these post-processing steps and consequently make the conventional production of high-quality Ti and TMCs tedious and expensive. As a great solution AM is utilized to simplify and speed up the manufacturing process and produce the complex near-net-shape Ti component without any further post-processing [98, 135, 136]. It should be emphasized that a significant difference in the melting point of the Ti matrix and reinforcements would result in different viscosities and melting/solidification behaviours, making their processability very complicated. Therefore, careful optimization should be carried out to properly melt and consolidate the TMCs.

Table 5 Summary of the effect of different reinforcements on the characteristics of the AMCs

Matrix	Reinforcement		Process	Features	Ref.
	Type	Content			
Al	$Al_{13}Fe_4$	–	DED	UTS: 205–240 MPa El: 1–3.8% Hardness: 70–85 HV	[122]
AlSi10Mg	Graphene	0.1–0.12 wt%	LPBF	YS: 22% increment (0.1 wt%) Hardness: 30% increment	[119]
	TiN	2 wt%	LPBF	COF: reduce to 0.43 Wear rate: $1.4 \pm 0.23 \times 10^{-3} mm^3 N^{-1} m^{-1}$ Hardness: 145 ± 4.9 HV	[123]
	TiB_2	–	DED	Porosity is decreased Vickers hardness is increased	[124]
	SiC	8.5 vol%	LPBF	Hardness: 2.27 GPa Elastic modulus: 78.94 MPa	[125]
	Graphene	0.5 wt%	LPBF	Wear resistance is improved COF is deceased Microhardness is increased	[126]
	CNT	0.5 wt%	LPBF	Microhardness: 154.12 HV Tensile strength: 420.8 MPa Elongation: 8.8%	[111]
	TiN	4 wt%	LPBF	UTS: 491.2 MPa YS: 315.4 MPa El: 7.5%	[127]
	SiC	–	LPBF	Relative density: 97.2% Microhardness: 218.5 $HV_{0.1}$ 19% reduction in COF	[128]
	TiN	2 wt%	LPBF	Microhardness: 138–145 $HV_{0.1}$ COF: 0.4–0.5	[123]
Al-3.5Cu-1.5 Mg-1Si	TiB_2	5 vol%	LPBF	YCS: 191 MPa UCS: ≈ 500 MPa	[129]

UTS ultimate tensile strength, *YS* yield strength, *El* elongation, *UCS* ultimate compressive strength, *CS* compressive strength, *COF* coefficient of friction, E_r reduced elastic modulus

Over the past decade, several reinforcements such as Cr_2O_3, TiN, TiO_2, SiC, Si_3N_4, TiB, TiB_2, Al_2O_3, Ti_5Si_3, boron particles, and carbonaceous nano-reinforcements such as CNTs, Gr have been used in the production of TMCs [133, 137]. It should be added that some of the reinforcements, such as TiC and TiB, are classified as ex situ, whereas some compounds like TiB_2 and SiC are considered as in situ reinforcements. In fact, in the in situ cases, the additive compounds react with the titanium, and the reaction product acts as reinforcement in the matrix (Fig. 11).

A summary of some most researched AM TMCs along with some of their important mechanical features is tabulated in Table 6.

Among all the aforementioned reinforcements, B, C, and their compounds like TiB and TiB_2 have attracted lots of attention in the production of TMCs. For instance, the considerable interested in TiB is mainly because of its unique

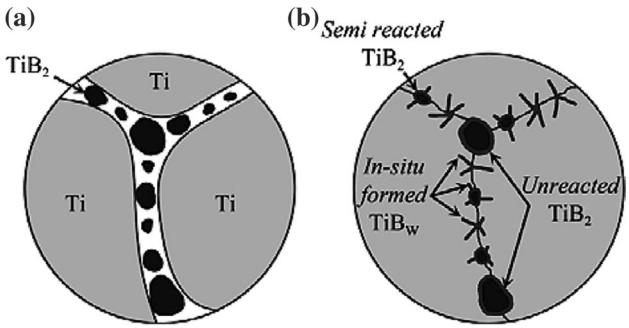

Fig. 11 Schematic representation of the formation of the TiB phase through an in situ reaction between Ti and TiB_2: **a** starting powder mixture showing the fine distribution of TiB_2 particles surrounding the larger Ti powders before sintering, **b** in situ formed needle-shaped TiB as well as semi-formed TiB, and unreacted TiB_2 particles during sintering [137]

Table 6 Summary of research on TMCs produced via different AM processes

Matrix	Reinforcement		Process	Features	Ref.
	Type	Content			
Ti-6Al-4V	–	–	DED	UTS: 1091.0 MPa El: 5.52(%)	[138]
	B_4C	5.3 vol%	DED	YS: 1190 MPa UTS:1190 MPa El: 0.3%	[33]
	TiC	0.9 vol%	DED	YS: 1080 MPa UCS: 1403 MPa CS: 28.2%	[139]
	TiC	15 vol%	DED	UTS: 1636 MPa True strain: 0.141	[139]
	TiC	13.8 vol%	EBM	UTS: 950 MPa El: 6.0%	[140]
	TiC_p	5–50 vol%	DED	Vickers Microhardness: 379.77–736.71	[141]
	HA	5 wt%	EBM	Tensile strength: 123 MPa El: 5.5% CS: 875 MPa Vickers hardness: 6.8 GPa	[142]
	CNTs	0.8 vol%	DED	YS: 1162 MPa UTS: 1255 MPa El: 3.2%	[143]
	TiB_2	–	DED	Hardness: 440–480 HV	[144]
	B_4C	1 wt%	LPBF	Vickers microhardness: 546 ± 7 HV UCS: 1747 ± 42 MPa Maximum true strain: 14.2 ± 1.2%	[145]
	B_4C	0.5 wt%	LPBF	Vickers microhardness: 458 ± 5 HV UCS: 1535 ± 18 MPa Maximum true strain: 19.3 ± 0.3%	

Table 6 (continued)

Matrix	Reinforcement		Process	Features		Ref.
	Type	Content				
Ti	TiB	8.35 vol%	LPBF	Vickers microhardness: 402 ± 7 HV		[146]
				UCS: 1421 ± 47 MPa		
				Maximum true strain: 17.8 ± 3.2%		
	TiC	5 wt%	LPBF	Density: 98.2%		[147]
				UTS: 914 MPa		
				El: 18.3%		
	TiB		LPBF	YS: 1103 MPa		[146]
				UTS: 1421 MPa		
				Vickers hardness: 402 HV		
	TiB		DED	YS: 940–1010 MPa		[148]
				UTS: 1016–1092 MPa		
				El: 26.5–36.5%		
	TiB		LPBF	Nanohardness: 4.75–3.33 GPa		[149]
				E_r: 153–122 GPa		
	TiB	2.5–7.5 wt%	LPBF	Harndess: 435 ± 14.7 $HV_{0.2}$ (for the sample with 7.5 wt% TiB)		[150]
	SiC	23.8 vol%	LPBF	Microhardness: 980.3 $HV_{0.2}$		[151]
				Friction coefficient: 0.2		
				Wear rate: 1.42×10^{-4} mm/Nm		
	SiC	20, 30, 40 wt%	LPBF	Hardness: 11–17 GPa Wear rate: 3.99×10^{-7}–9.51×10^{-7} g/Nm		[152]
	SiC	30 wt%	LPBF			[153]
	SiC		DED	300 W, 20 mm/s	Wear rate: 6.60×10^{-4} g/Nm	[154]
					Microhardness: 976 ± 71 HV	
				400 W, 10 mm/s	Wear rate: $511\pm63\times10^{-4}$ g/Nm	
					Microhardness: 1167 ± 194 HV	

properties and stability in the TMCs. In fact, the very low (< 0.001 at%) solubility of B in Ti is the reason for its stability in the Ti matrix. Moreover, the coefficient of thermal expansion of TiB, which is very close to the Ti matrix, reduces the formation of residual stresses in the final TMCs. On the other hand, in situ produced TiB particles form a good and clean interfacial bonding with the Ti matrix [155]. Attar et al. [146] produced a Ti-TiB composite through the LPBF process in order to study its processability, microstructure, and mechanical performance. They found that the irregular TiB_2 particles reacted with Ti, and consequently, needle-shaped TiB particles were formed (Fig. 12). In fact, Ti could react with TiB_2 through an in situ reaction by either diffusional removal of B from TiB_2 into the titanium matrix or via melting and formation of TiB during the solidification. The formation of TiB needles increased the microhardness, YS, and compressive strength of the TMCs from 261 Hv, 560 MPa, and 1136 MPa to 402 Hv, 1103 MPa, and 1421 MPa, respectively [146].

Attar et al. [146] also studied the processability of Ti-TiB_2. For this, at first, they milled the CP-Ti and TiB_2 powder blend for 2 h to achieve a nearly spherical powder mixture for the LPBF process. Thereafter, the composite powder was processed using different energy densities starting from 120 J/mm^3, which was the optimum energy density for LPBF of CP-Ti. It was found that the samples produced using energy densities higher than 120 J/mm^3 were rather porous. Furthermore, when the laser power increased with

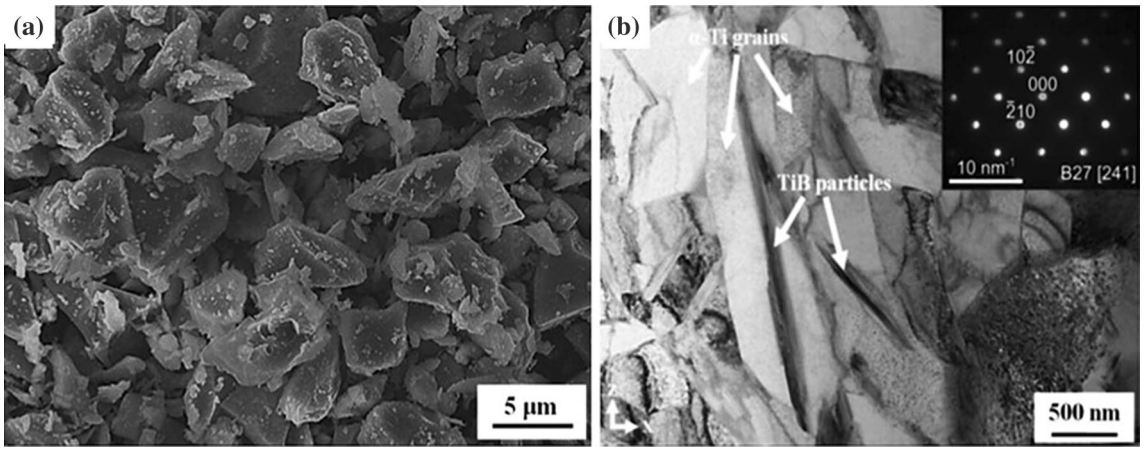

Fig. 12 **a** Particle shape and morphology of the starting TiB_2 powder, **b** TEM images showing the microstructures of the SLM-processed Ti-TiB composite showing needle-shaped TiB particles embedded in a matrix of α-Ti grains with lamellar structure [146]

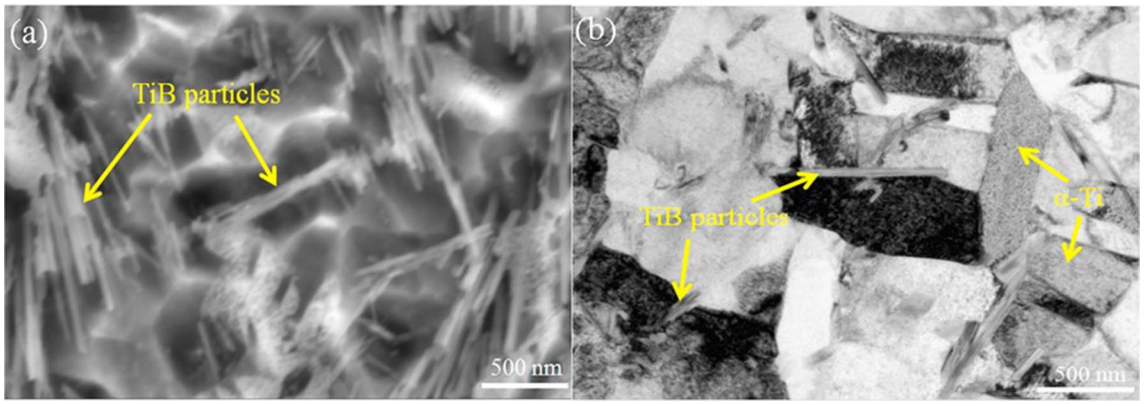

Fig. 13 **a** SEM and **b** bright-field TEM images of Ti-TiB composite materials after LPBF processing [149]

the laser energy density being constant, the samples were consolidated up to 99.5%. In another work, Attar et al. [149] studied the nanoindentation and wear properties of Ti-TiB composites produced via the LPBF process. In their work, a uniform distribution of needle-like TiB particles was found across the α-Ti matrix (Fig. 13) that resulted in higher hardness, elastic modulus, and wear resistance in comparison with those of pure Ti [149].

According to Attar et al. [149], this type of microstructure can be formed due to the presence of B and high cooling rates during the solidification step. It is also interesting to point out the formation α-Ti instead of α' martensite in the case of TMCs reinforced by TiB_2 was found to be as a consequence of B that reduced the martensitic transformation temperature [156]. Attar et al. [157] further compared the microstructure and mechanical properties of Ti-TiB_2 composites produced via casting and LPBF processes. They found that since the LPBF process is a rapid solidification process the heating/cooling rates in this process are very high and, as a consequence, the time for grain growth is much shorter than that of the casting, and this difference results in the formation of much finer TiB needles in the LPBF TMCs. Xia et al. [158] produced a TMC reinforced by B_4C using the LPBF process. Interestingly, they revealed a novel microstructure, including in situ formed needle-like TiB and granular TiC phases around the B_4C particles (Fig. 14) so that a high microhardness of 577.1 $HV_{0.2}$ resulted. Moreover, it was found that at higher laser powers, the size of in situ formed phases (TiB and TiC) increased due to the increase in the input energy, leading to the decrease in microhardness of the TMC samples.

In another research carried out by Li et al. [145], the effect of B_4C addition on the microstructure evolution, compressive properties, hardness, and fracture mechanisms of LPBF Ti-6Al-4V composites was studied. According to their results, there was a maximum increment of about 45% and 26%, respectively, in Vickers microhardness and UCS as compared to those of the Ti-6Al-4V matrix (Fig. 15a).

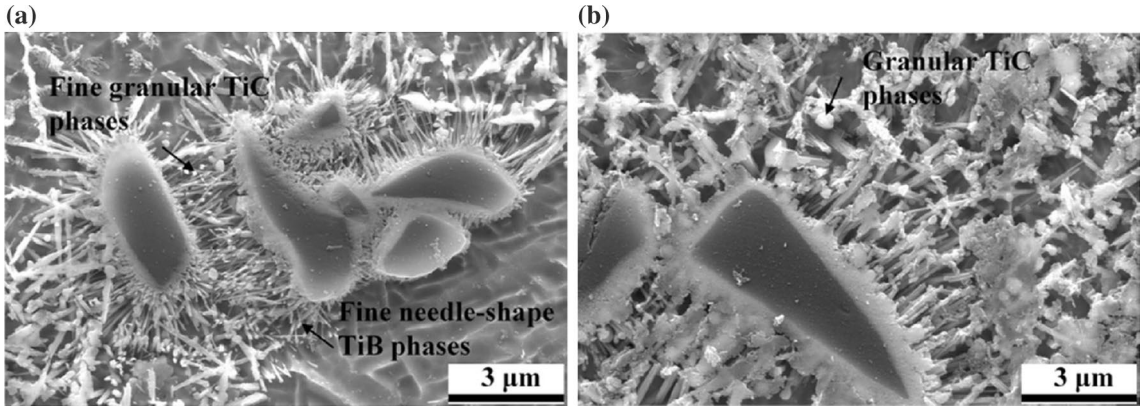

Fig. 14 High-magnitude morphologies of microstructures located on the top surface of LPBF-processed B_4C/Ti composite parts at different laser power: **a** 125 W, 800 mm/s; **b** 150 W, 800 mm/s [158]

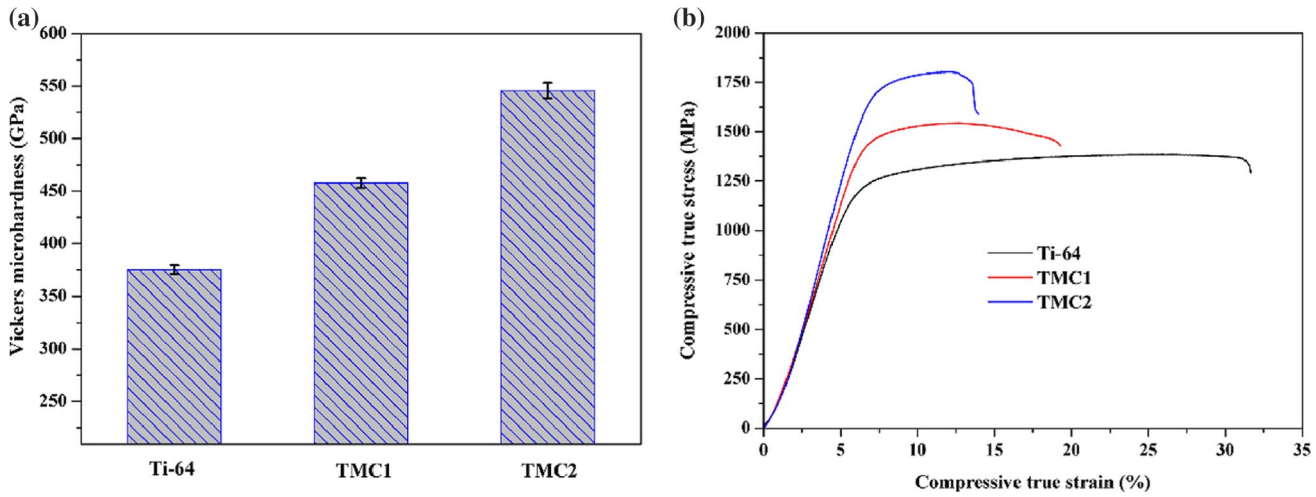

Fig. 15 Vickers microhardness and typical compressive true stress–strain curves of Ti-64, 0.5 wt% B_4C (TMC1) and 1.0 wt% B_4C (TMC2) [145]

They revealed that by addition of B_4C, there was a remarkable increase in the average nanohardness from 4.93 GPa to 5.46 GPa for 0.5 wt% B_4C and to 6.11 GPa when 1.0 wt% B_4C was added. This increase in micro- and nanoscale hardness can be attributed to the simultaneous effect of in situ formed reinforcements and fine LPBF microstructure of the Ti matrix. Moreover, a gradual improvement in Young's modulus was observed with an increment of B_4C reinforcement particles. According to Fig. 15b, the UCS of the TMC was significantly enhanced in the presence of B_4C from 1384 MPa (Ti-6Al-4V) to 1535 MPa (0.5 wt% B_4C) and to 1747 MPa (1.0 wt% B_4C), respectively. In general, improvements in the mechanical features can be attributed to three main strengthening mechanisms, namely second-phase strengthening, grain refinement strengthening as well as solid solution one.

Pouzet et al. [33] studied the microstructural and mechanical characteristics of Ti-6Al-4V/B_4C composite fabricated via the DED process. They reported significant grain reinforcement for TMCs even in samples with low B_4C contents due to an enhancement in grain nucleation effect by TiB needles. As can be seen in Fig. 16, there was an enhancement in Vickers hardness (about 10–15%) and Young's modulus (10%) for all the B_4C/Ti-6Al-4V samples in a wide temperature range of 20–600 °C.

Pouzet et al. [33] also showed that the UTS (≈1000–1100 MPa) and elongation of Ti-6Al-4V were higher in samples machined in the direction of laser scanning (*L*) (4–5%) in comparison with those machined in along the layer growth (*T*) (about 1%) (Fig. 17a). As can also be seen in Fig. 17b, by addition of 1.5 wt% B_4C, there was a decrease in the ductility of samples, and the UTS values decreased from

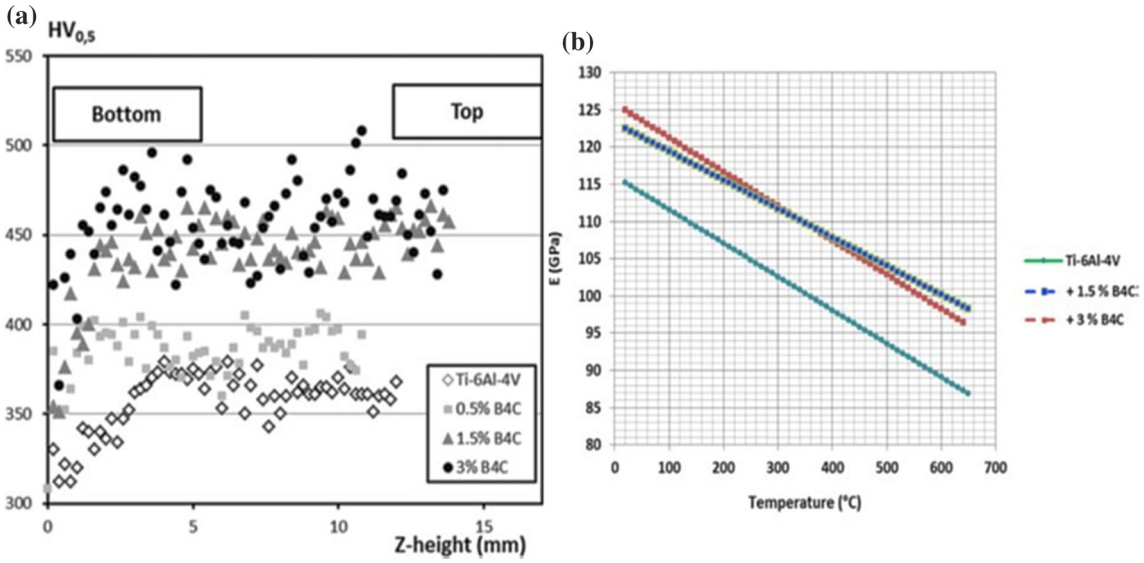

Fig. 16 Mechanical properties of Ti-6Al-4V composite in the presence of the various amount of B_4C: **a** Vickers hardness, **b** Young's modulus [33]

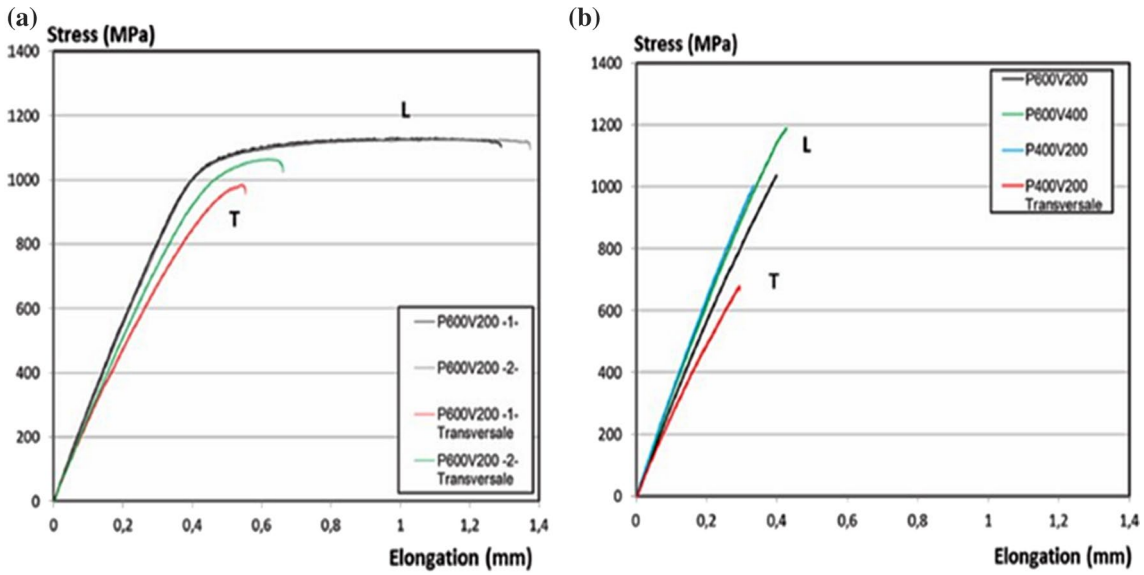

Fig. 17 Room temperature tensile stress–strain curves of **a** Ti-6Al-4V alloy; **b** Ti-6Al-4V-1.5wt% B_4C [33]

1000–1200 MPa in the L direction to 700 MPa in the T direction (Fig. 17b).

At higher temperatures (500 °C), the composite showed better properties as compared to Ti-6Al-4V with approximately similar results obtained for two directions of *L* and *T*. The UTS increased up to 830 MPa (Fig. 18a, b), whereas the elongation of the composites decreased (6–9%). The decrease in ductility of the composites was confirmed by the SEM micrograph of the fracture surfaces (Fig. 19). The classical ductile behaviour of Ti-6Al-4V and brittle inter-granular properties of Ti-6Al-4V-1.5wt% B_4C are illustrated in Fig. 19a and b, respectively [33].

Terrazas et al. [142], for the first time, produced a novel TMC reinforced by Hydroxyapatite (HA) using the EBM process. In that work, in addition to the bulk samples, they also fabricated four various lattice structures with various densities, compression strengths, and Young's moduli, respectively, being in 0.68–1.12 g/cm^3, 3–11 MPa and 2.9–8.0 GPa (Fig. 20). It was found that in both bulk and lattice samples, HA particles segregated in Ti-6Al-4V grain boundaries and also α platelet boundaries. This

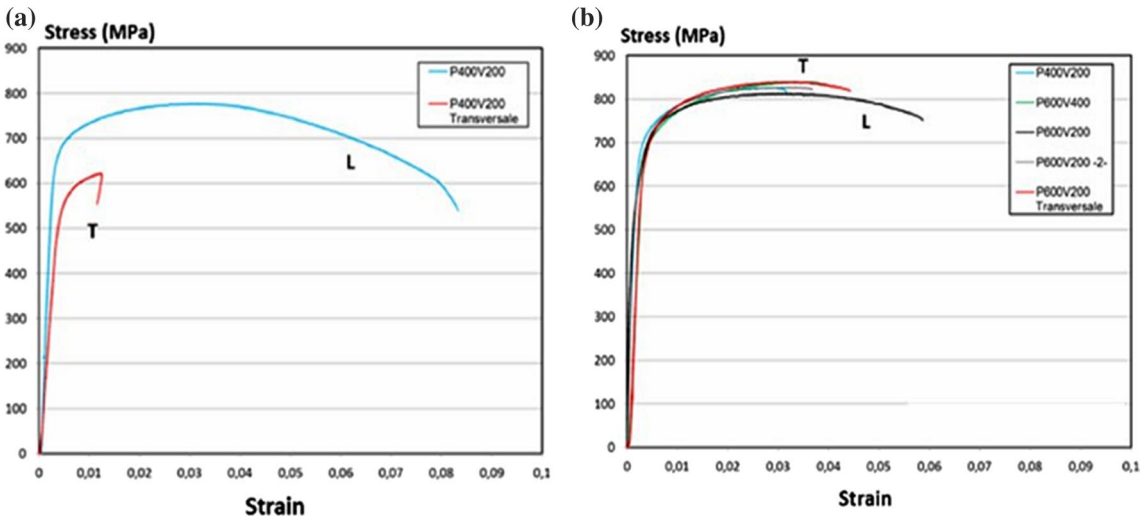

Fig. 18 Tensile stress–strain curves of **a** Ti-6Al-4V; **b** Ti-6Al-4V-1.5 wt%B_4C, at 500 °C [33]

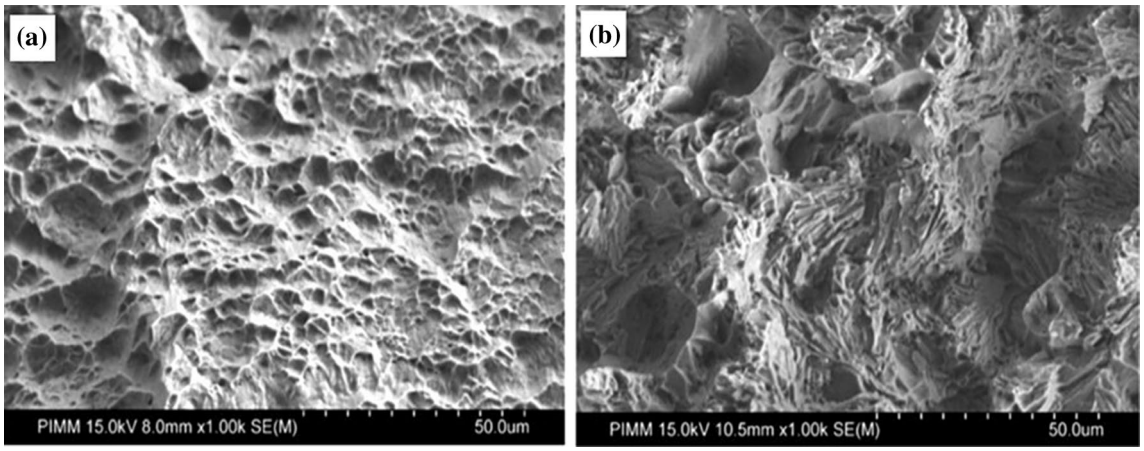

Fig. 19 SEM analysis of fracture surface of **a** Ti-6Al-4V; **b** Ti-6Al-4V-1.5wt% B_4C, at 500 °C [33]

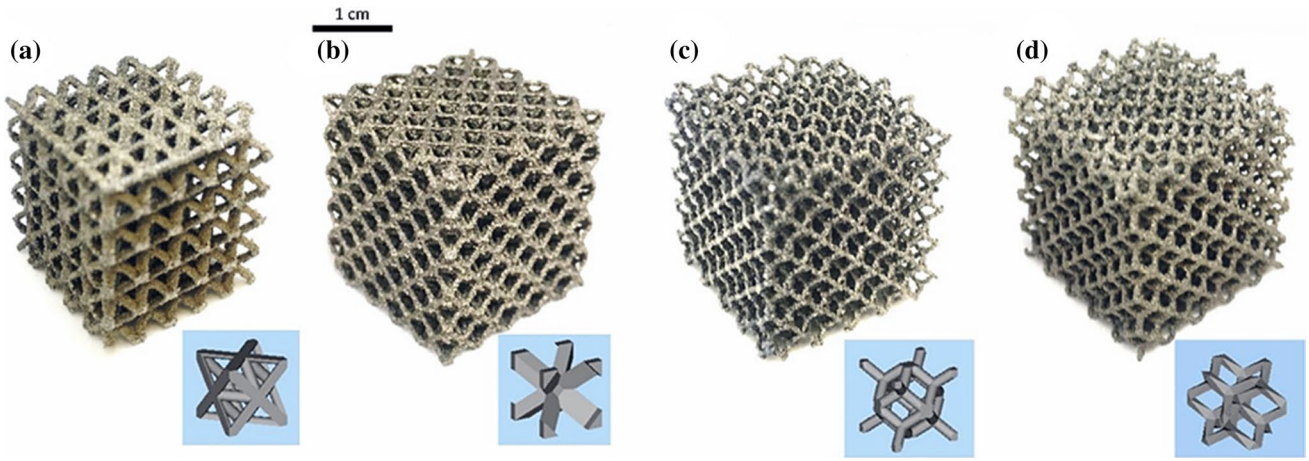

Fig. 20 Comparison of open-cellular, mesh design models (unit cells) and corresponding EBM-fabricated mesh structures in decreasing order of density. **a** Octet truss, **b** G structure 3 (G3), **c** Rhombic dodecahedron, **d** Dode medium [142]

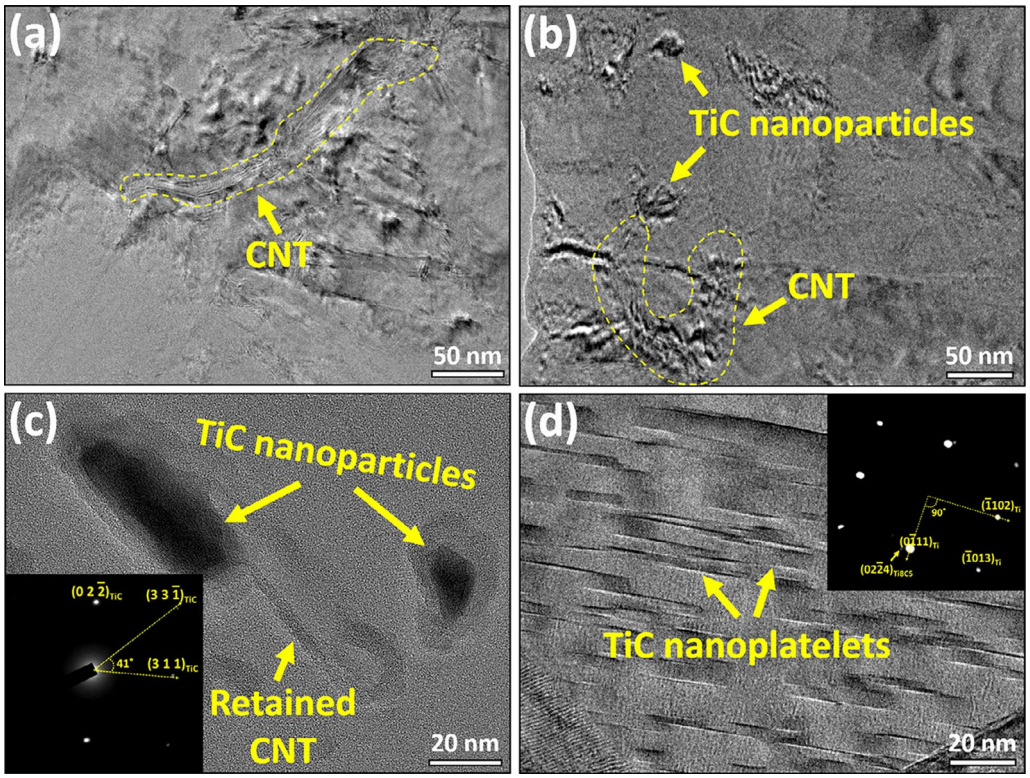

Fig. 21 TEM images of the printed composite: **a** bright-field (BF) micrograph, **b** morphology and distribution of reinforcements, **c** morphology of reinforcements replicated from the matrix and the SAED pattern of a TiC nanoparticle, **d** morphology and distribution of TiC nanoplatelets and the corresponding SAED pattern [143]

segregation of HA in grain boundaries was found to be the source of shear-to-brittle behaviour of the TMCs during the mechanical testing.

Their work showed that through the optimization of process parameters and modification of the feedstock materials, it would be possible to produce bulk and open-cellular structures that can be used in the manufacturing of new bone scaffolds and implants in the biomedical field.

As regards the carbonaceous reinforcements, recently, Liu et al. [143] studied the processability of the Ti-6Al-V-CNTs composites by the LPBF method. The microstructure TMCs reinforced by CNTs shown in Fig. 21 illustrated that TiC nanoparticles and nanoplatelets were formed through the interfacial reaction and dissolution–precipitation mechanisms, respectively, whereas some CNTs were remained untouched (Fig. 21a), showing their good chemical stability. As can be seen in Fig. 21b, some nanoparticles were distributed around the remained CNTs indicating an interfacial reaction between the CNTs/Ti. Figure 21c shows retained CNTs with a well-crystallized structure. Selected area electron diffraction (SAED) analysis confirms the formation of the TiC nanoparticles (with FCC structure) around the retained CNTs (Fig. 21c). Furthermore, it was revealed that the TiC nanoparticles were uniformly dispersed within the in α-Ti (Fig. 21d).

Their mechanical evaluation clearly showed that through the incorporation of CNTs as reinforcement, the UTS and YS of the composites increased from 1078 to 1255 MPa and from 964 to 1162 MPa compared to those of the Ti-6Al-4V alloy (Fig. 22a). It was while the elongation decreased approximately by 3.2% as a consequence of synergy between bridge enhancement of TiC nanoplatelets and load transfer from matrix to CNTs. Figure 22b demonstrates a typical dimple and quasi-cleavage morphology, indicating a mixed fracture mode as the major feature of tensile samples. Furthermore, strengthening mechanisms of CNTs and TiC are demonstrated in Fig. 22c.

In the whole, Ti base alloys are among the most promising alloy groups having the capacity of making a drastic change in properties by including a reinforcing phase. Featured with a high strength/weight ratio, producing TMCs gives added applicability to the Ti base matrix. AM of TMCs, on the other hand, has enhanced the mechanical properties of the TMCs even more than before, thanks to the AM rapid solidification nature. The results published by the literature on AM TMCs indicate carbides and borides are among the most promising materials used

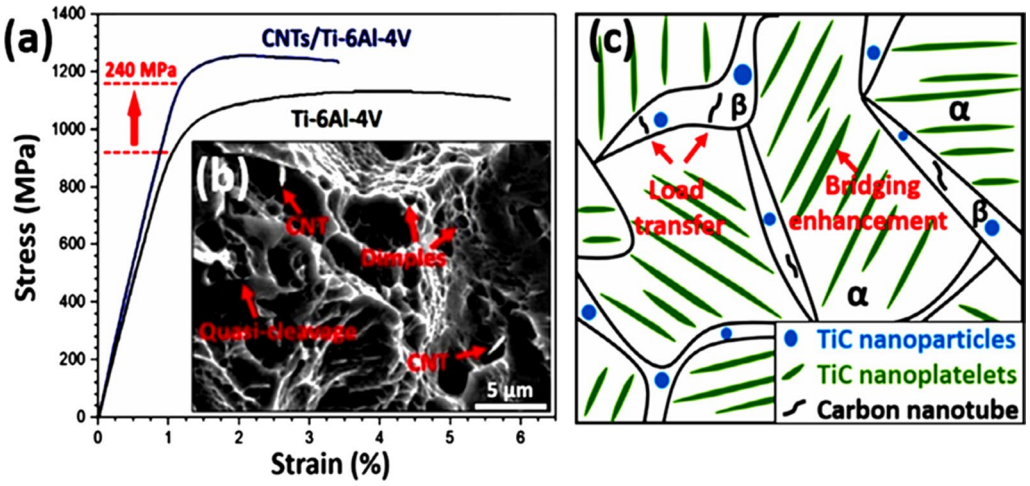

Fig. 22 **a** Tensile stress–strain curves of as-printed Ti-6Al-4V alloy and composite, **b** SEM fractography of the tensile fractured composite, **c** schematic illustration of the strengthening [143]

as reinforcing materials. Though multiple researches are published so far, there are still challenges to deal with. For instance, more reinforcing materials can be examined in terms of evaluating their processability, addition to the mechanical properties of the final composites. Moreover, given the flexibility of the method, biocompatible TMCs with complex geometries can be considered as a promising research area.

3.2.3 Other Matrix Composites

Though the literature is not limited to the AM AMCs and TMCs, the number of publications employing other metals as the matrix is still negligible. Some of the most promising works are tabulated in Table 7. AlMangour et al. [29] produced 316L stainless steel/TiB_2 nanocomposites via the LPBF method by adding TiB_2 nanoparticles to the 316L

Table 7 Some of the non-Ti/Al-based MMCs produced via different AM processes

Composite	Reinforcement		Process	Features	Ref.
	Type	Content			
316L stainless steel	TiB_2 (nanoparticles)	0–10 vol%	LPBF	CYS = 980.9 ± 10.9 MPa (for samples with 10 vol% TiB_2)	[160]
316L stainless steel	SiC	4–16 wt%	DED	Microhardness: 362–974 HV Corrosion current density: Increased Corrosion resistance: Decreased	[159]
Stainless steel	V	12 wt%	DED	Microhardness: 521 ± 9–603 ± 12 HV Ware rate: 5.011×10^{-6} mm^3/N m	[161]
316L stainless steel	TiN	1–10 wt%	LPBF		[162]
316L stainless steel (coating)	TiC	20–80 wt%	DED		[163]
Inconel 625	SiC, Al_2O_3, TiC	5 wt%	DED	IN625/SiC: 130% increase of hardness, increase of porosity and cracking IN625/Al_2O_3: No significant change in density and hardness IN625/TiC: 30% increase of hardness	[164]
Inconel 625	TiC (nanoparticles)	4 wt%	LPBF	Enhanced oxidation properties	[165]
Inconel 718	TiC (nanoparticles)	0.5 wt%	LPBF	Tensile strength: 1370 MPa (after ageing heat treatment)	[166]
(HY282) superalloy	SiC		DED	Graded microstructure Hardness gradient: from 200 HV (bottom) to ~ 800 HV (top)	[32]
Copper	Diamond	25 vol%	DED	Relatively dense: 96% Thermal conductivity: 330 W/m K	[167]
Ti-6Al-4V	HA	5 wt%	EBM	Tensile strength: 123 MPa Maximum compressive strength: 875 MPa	[142]

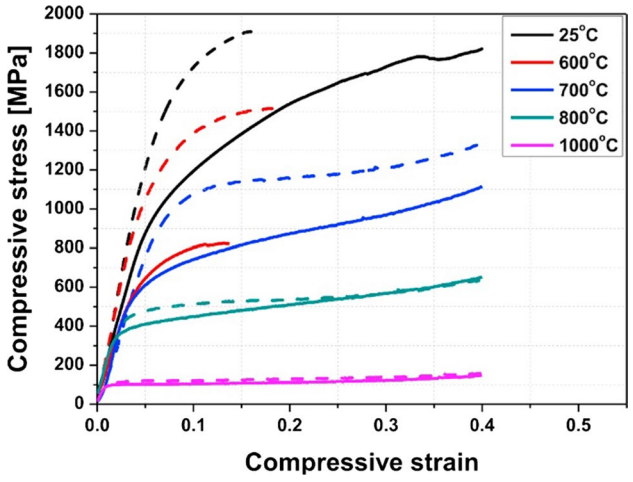

Fig. 23 Compressive stress–strain curves of 316L composites containing 5 vol% (solid) and 10 vol% (dashed) TiB_2 nanoparticles [160]

stainless steel powder blend. The authors reported improved compressive strength of the samples in a temperature range (Fig. 23). More significantly, the results suggested a "microsegregation strengthening mechanism" as an effective strengthening mechanism besides the conventional ones. Wu et al. [159] employed DED for producing reinforcing 316L stainless steel matrix with different amounts of SiC powders. Their results showed SiC as being highly influential in increasing the hardness and corrosion resistance of the composites (Fig. 24).

Improvement of the mechanical and corrosion properties in work by Wu et al. [159] was attributed to the effect of SiC on the physical and mechanical characteristics of the matrix. It should be noted that the SiC reinforcing particles not only refined the solidification microstructure of the matrix but also reportedly led to a microstructural evolution from single γ-(FeCrNi) phase for 4 wt% SiC dispersed MMC to γ-(FeCrNi) + α-(FeCrNi) + SiC phases for the 8, 12, and 16 wt% SiC dispersed MMCs. The latter change was attributed to the tensile stress stemming from the difference in the coefficient of thermal expansion between SiC ceramic reinforcement and the γ-(FeCrNi) matrix in the MMCs. Li et al. [161] improved the mechanical properties of stainless steel by mixing gas-atomized stainless steel powders with V powders and produced samples via DED method. The in situ produced VC phase acted as heterogeneous nucleation sites for α-Fe and carbides of chromium, leading to the enhancement of the mechanical properties (Fig. 25).

Cooper et al. produced three different Inconel 625 matrix composites via the DED method by adding ceramic reinforcing particles, namely SiC, Al_2O_3, and TiC [164]. According to the results shown in Fig. 26, the introduction of silicon carbide particles increased the hardness by 130% while it also increased porosity and cracking. From the other hand, while Al_2O_3 had no significant effect on density and hardness of the sample, TiC led to a 30% increased hardness along with an acceptable density.

Biomaterials with low degradation rate are one of the main challenges in clinical applications. Since the degradation rate of pure iron (Fe) as a promising candidate biodegradable metal is too low, in 2020, Zhao et al. [168] prepared iron-graphene oxide (0.4–1.6 wt% GO) composites by LPBF process to enhance its degradation rate. They found that the microstructure, hardness, corrosion, and degradation rate were significantly affected in the presence of graphene oxide as a reinforcement. The authors recommended 0.8 wt% of GO to achieve the maximum value of density and hardness as well as corrosion and degradation rate along with a good cytocompatibility. The faster

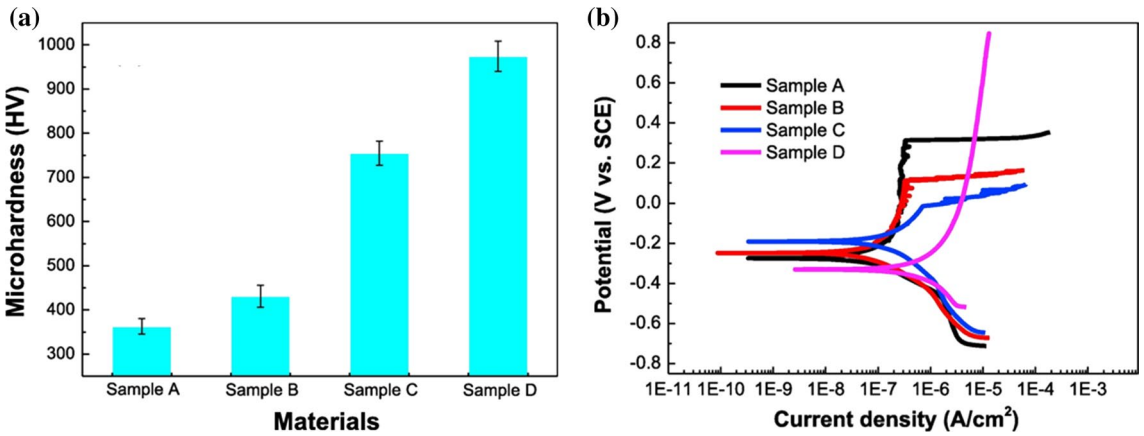

Fig. 24 Change in **a** microhardness, **b** potentiodynamic polarization curves of 316L stainless steel SiC composites with the amount of SiC. The polarization test is carried out in 3.5 wt% NaCl solution while being exposed to air, and samples A, B, C, and D contain 4, 8, 12, and 16 wt% SiC, respectively [159]

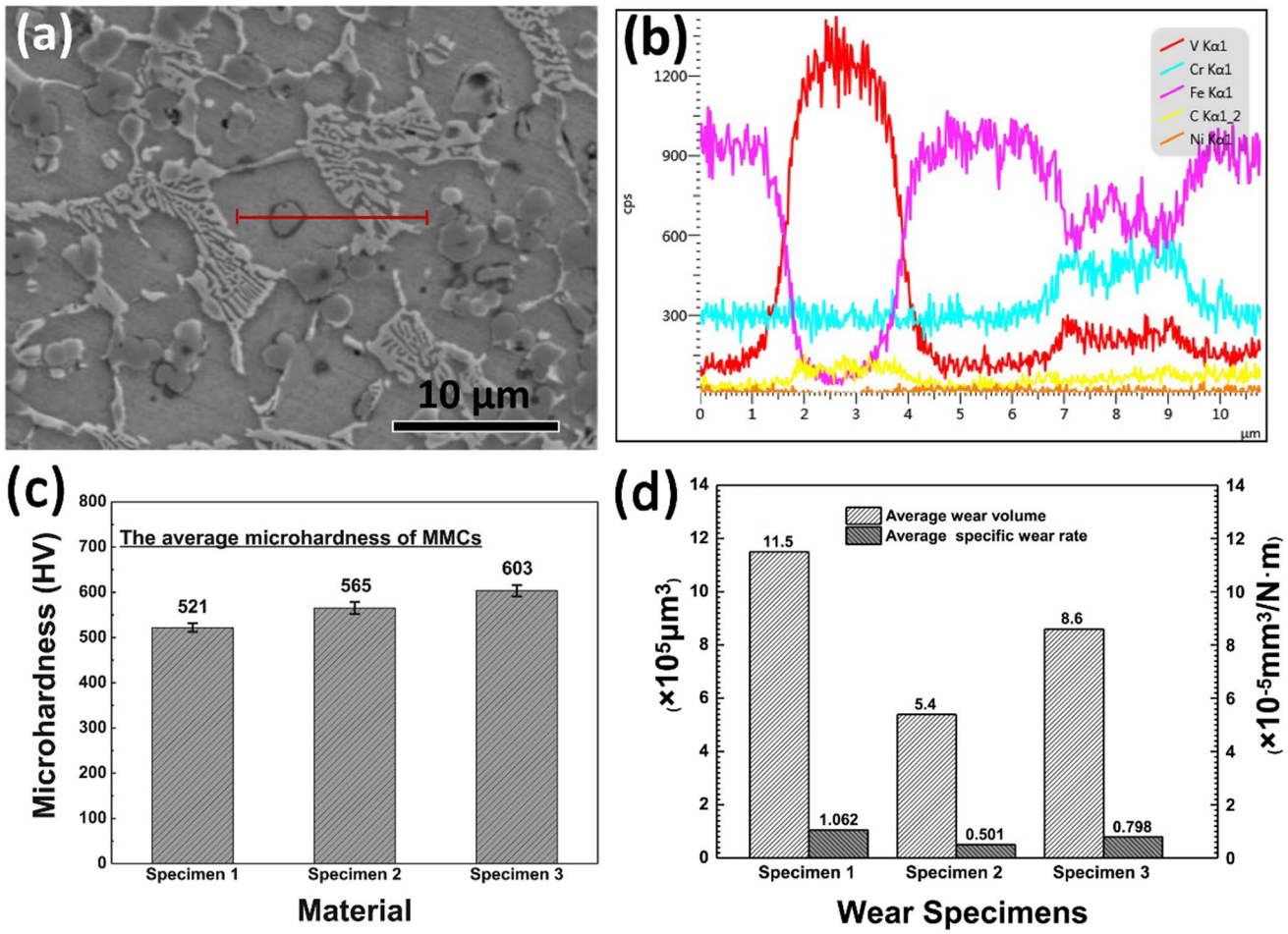

Fig. 25 **a** SEM image of the stainless steel composite reinforced with 12 wt% V, **b** EDS line of the VC precipitate, **c** microhardness of the samples, **d** the wear behaviour of the samples. Specimens 1, 2, and 3, respectively, contain 9, 12, and 15 wt% V [161]

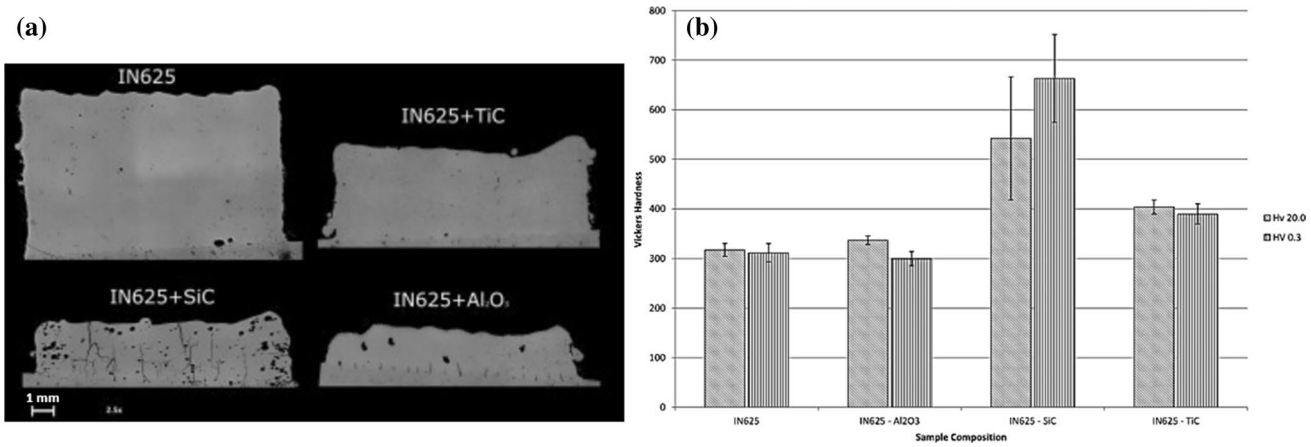

Fig. 26 **a** Optical microscope photographs of monolithic and composite sections, at 2.5×magnification, **b** Vickers hardness of the monolithic and composite samples [164]

degradation rate of composites compared to pure Fe can be described by a microgalvanic corrosion mechanism. The literature review indicates just a handful of works are dedicated to the production of MMCs using the EBM method. Hence, there is a prospect for the fabrication of a variety of metal/ceramic composites applying the LPBF additive manufacturing process.

4 Main Challenges

Although AM techniques are able to fabricate complex components besides providing freedom of design and customization, they suffer from some disadvantages such as high costs, limited applications in the manufacturing of large structures and mass production, inferior and anisotropic mechanical properties, and limitation of feedstock materials. Hence, further research, technological development, and improvement of materials and methods are necessary to overcome some of these problems. As an example, in comparison to traditional techniques (such as casting, extrusion, fabrication, or injection moulding), AM of components is typically more time-consuming. In particular, AM methods such as LPBF and SLS are of high resolution making the processing costly and time-consuming. High cost and long process time can be considered the main challenges of AM techniques, limiting the mass production of parts that can be fabricated by traditional methods with reasonable time and cost [90]. In spite of this, AM methods can especially be cost-effective in the case of customized products with complicated geometries such as the lattices used in medical applications [169].

The homogenous distribution of the reinforcement in the matrix can be considered as a major challenge for liquid-based MMC production techniques. AM methods, however, are capable of providing a uniform and customized distribution of second phase particles inside the matrix. This is probably the most significant feature of AM MMCs, which can be achieved by suitable feedstock preparations such as conventional jar milling of the blends or decorating the parent particles with tiny particles of the reinforcement phase. Furthermore, the amount of the second phase particles can simply be tailored towards the build direction in the case of the DED method, where the reinforcing particles can be fed into the melt pool via separated nuzzles.

Going through the literature, it is evident that finding the optimized sets of parameters creating reproducible properties is a concern as regards the AM MMCs. Although the method is fundamentally able to produce a wide range of composites given its additive nature and the concentrated heat source utilized in the method, employing suitable process parameters is of vital importance, especially for the in situ composites. The latter involves in-process time-dependent reactions marking the importance of the input energy. Moreover, due to the fast cooling rate of the AM process, the addition of secondary ceramic particles may increase the vulnerability to cracking, which indicates that the type, morphology, and amount of the second phase material need to be carefully selected according to the possible in situ reactions, brittle phases and the crack vulnerability of the metallic matrix. Despite the recent efforts by the researchers, the range of materials used to produce AM MMCs is still limited. This limitation is much more severe in the case of EBM technology. In fact, in the EBM systems, there are two limitations for using submicrometric or nanometric materials: vacuum pumps and powder sensors. Since the fine reinforcements can negatively affect the performance of these parts, it not recommended to use them inside the EBM machines. Finally, in comparison with the conventional composites, lack of basic standards for the AM of MMCs, the challenges regarding the scale-up of the AM MMCs, lack of knowledge regarding the preparation of suitable feedstock, and the production costs of the AM MMCs are among the main challenges that the AM technology is faced with.

5 Conclusions

Recent works on the production of metallic matrix composites produced by the additive manufacturing method are reviewed in this paper. Methodology, processability, and major results were investigated, and the following can be concluded:

1. As compared to the conventional methods, AM provides a flexible, clean, and near-net-shape production method of MMCs. The capability of AM to produce complicated geometries with a uniform distribution of reinforcements is probably the most interesting advantageous of AM over conventional methods. Needless to mention that AM gives the possibility of creating a gradient of second phase particles along the build direction, a significant feature that adds to the flexibility of the AM method in producing MMCs.
2. The literature review indicates the aluminium- and titanium-based composites are among the most studied types of AM MMCs. Various ceramic particles are utilized as reinforcement materials. That said, some limited works are dedicated to stainless steel-based or superalloy-based composites. Although AM is fundamentally categorized as a rapid solidification process, the results show that the method can be employed for producing in situ composites, where the reinforcement

is produced as a result of a reaction between the matrix and the secondary particles. On the other hand, fast cooling condition creates an ultrafine microstructure, further enhancing the mechanical properties of the MMCs.

3. Suitable composite feedstock with the appropriate size and flowability can be considered a key challenge regarding the AM MMCs. Despite the fact that dozens of papers are published so far, more works should be carried out aimed at developing feedstocks specially designed for AM MMCs.
4. A significant difference in the physical properties of the matrix and the reinforcements, including the melting temperature and the coefficient of expansion, may create processability challenges such as cracks and unwanted reactions.
5. Other arising issues regarding the AM MMCs can be the difficulties regarding the scale-up of the AM MMCs, lack of knowledge regarding the preparation of suitable feedstock, size limitations, and the production costs of the AM MMCs. More research is required to address the aforementioned production issues along with the mechanisms and properties of AM MMCs in an in-depth manner.

Funding Open access funding provided by Politecnico di Torino within the CRUI-CARE Agreement.

References

[1] M. Dadkhah, A. Saboori, P. Fino, Materials (Basel) **12**, 2823 (2019)
[2] A. Saboori, S.K. Moheimani, M. Dadkhah, M. Pavese, C. Badini, P. Fino, Metals (Basel). **8**, 172 (2018)
[3] M.Yakout, M. A. Elbestawi, in *6th International Conference on Virtual Machining Process Technology* (Montréal, 2017)
[4] S.K. Moheimani, M. Dadkhah, M.H. Mosallanejad, A. Saboori, Metals (Basel) **11**, 125 (2021)
[5] W.H. Yu, S.L. Sing, C.K. Chua, C.N. Kuo, X.L. Tian, Prog. Mater. Sci. **104**, 330 (2019)
[6] S.A. Sajjadi, H.R. Ezatpour, H. Beygi, Mater. Sci. Eng. A **528**, 8765 (2011)
[7] S.A. Sajjadi, H.R. Ezatpour, M.T. Parizi, Mater. Des. **34**, 106 (2012)
[8] A. Saboori, E. Padovano, M. Pavese, C. Badini, Materials (Basel) **11**, 171 (2018)
[9] A. Saboori, E. Padovano, M. Pavese, H. Dieringa, C. Badini, Mater (Basel) **10**, 1380 (2017)
[10] F. Barati, M. Latifi, E. Moayeri far, M.H. Mosallanejad, A. Saboori, Materials (Basel) **12**, 3976 (2019)
[11] J.P. Tu, W. Rong, S.Y. Guo, Y.Z. Yang, Wear **255**, 832 (2003)
[12] R.R. Zheng, Y. Wu, S.L. Liao, W.Y. Wang, W.B. Wang, A.H. Wang, J. Alloys Compd. **590**, 168 (2014)
[13] K. Chu, Z. Liu, C. Jia, H. Chen, X. Liang, W. Gao, J. Alloy. Compd. **490**, 453 (2010)
[14] A. Saboori, R. Casati, A. Zanatta, M. Pavese, C. Badini, M. Vedani, Powder Metall. Met. Ceram. **56**, 647 (2018)
[15] S. Dadbakhsh, R. Mertens, L. Hao, J. Van Humbeeck, J.P. Kruth, Adv. Eng. Mater. **21**, 1801244 (2019)
[16] A.K. Ghosh, Solid State Processing, in *Fundamentals of Metal-Matrix Composites*. ed. by S. Suresh, A. Mortensen, A. Needleman, Butterworth-Heinmann,1993), pp. 23-41
[17] A. Saboori, M. Dadkhah, P. Fino, M. Pavese, Metals (Basel). **8**, 423 (2018)
[18] J. Savolainen, M. Collan, Addit. Manuf. **32**, 101070 (2020)
[19] C. W. Hull, U.S. Patent 4,575,330 A, March 1986
[20] J.S. Gero, M.L. Maher, in *Third International Round Table Conference on Computational Models of Creative design*, (Key Centre of Design Computing at the University of Sydney, Heron Island, Queensland, Australia, 1995)
[21] C. Chu, G. Graf, D.W. Rosen, Comput. Aided Des. Appl. **5**, 686 (2008)
[22] O. Ivanova, C. Williams, T. Campbell, Rapid Prototyp. J. **19**, 353 (2013)
[23] J.O. Milewski, Understanding Metals for Additive Manufacturing, in *Additive Manufacturing of Metals*, (Springer International Publishing, 2017), pp. 7-33
[24] P. Wu, J. Wang, X. Wang, Autom. Constr. **68**, 21 (2016)
[25] J.W. Stansbury, M.J. Idacavage, Dent. Mater. **32**, 54 (2016)
[26] M.S.K.K.Y. Nartu, S.A. Mantri, M.V. Pantawane, Y.H. Ho, B. McWilliams, K. Cho, N.B. Dahotre, R. Banerjee, Scr. Mater. **183**, 28 (2020)
[27] C. Doñate-Buendía, F. Frömel, M.B. Wilms, R. Streubel, J. Tenkamp, T. Hupfeld, M. Nachev, E. Gökce, A. Weisheit, S. Barcikowski, F. Walther, J.H. Schleifenbaum, B. Gökce, Mater. Des. **154**, 360 (2018)
[28] M.P. Behera, T. Dougherty, S. Singamneni, Procedia Manuf. **30**, 159 (2019)
[29] B. AlMangour, D. Grzesiak, J.M. Yang, Powder Technol. **309**, 37 (2017)
[30] D. Gu, H. Wang, G. Zhang, Metall. Mater. Trans. A **45**, 464 (2014)
[31] D. Gu, C. Ma, M. Xia, D. Dai, Q. Shi, Engineering **3**, 675 (2017)
[32] A. Ramakrishnan, G.P. Dinda, Mater. Des. **179**, 107877 (2019)
[33] S. Pouzet, P. Peyre, C. Gorny, O. Castelnau, T. Baudin, F. Brisset, C. Colin, P. Gadaud, Mater. Sci. Eng. A **677**, 171 (2016)
[34] A. Saboori, D. Gallo, S. Biamino, P. Fino, M. Lombardi, Appl. Sci. **7**, 883 (2017)
[35] A. Saboori, A. Aversa, G. Marchese, S. Biamino, M. Lombardi, P. Fino, Appl. Sci. **9**, 3316 (2019)
[36] N. Shamsaei, A. Yadollahi, L. Bian, S.M. Thompson, Addit. Manuf. **8**, 12 (2015)
[37] A. Standard, F2792. 2012. Standard terminology for additive manufacturing technologies, ASTM F2792–10e1. (2012)
[38] N. Guo, M.C. Leu, Front. Mech. Eng. **8**, 215 (2013)
[39] A. others Standard, Standard terminology for additive manufacturing technologies, ASTM Int. F2792–12a. (2012)

[40] M.H. Mosallanejad, B. Niroumand, A. Aversa, D. Manfredi, A. Saboori, J. Alloys Compd. **857**, 157558 (2020)
[41] F.I. Azam, A.M. Abdul Rani, K. Altaf, T.V.V.L.N. Rao, H.A. Zaharin, in, *IOP Conference Series: Materials Science and Engineering*, vol. 328 (2018), p. 012005
[42] M.H. Mosallanejad, B. Niroumand, A. Aversa, A. Saboori, J. Alloys Compd. **872**, 159567 (2021)
[43] I. Yadroitsev, P. Bertrand, I. Smurov, Appl. Surf. Sci. **253**, 8064 (2007)
[44] S. Bremen, W. Meiners, A. Diatlov, Laser Tech. **9**, 33 (2012)
[45] E. Yasa, J. Kruth, Adv. Prod. Eng. Manag. **6**, 259 (2011)
[46] W. Sames, F. Medina, W. Peter, S. Babu, R.R. Dehoff, in, *8th International Symposium on Superalloy 718 and Derivatives*, pp. 409–423
[47] X. Zhang, C.J. Yocom, B. Mao, Y.L. Liao, J. Laser Appl. **31**, 31201 (2019)
[48] Y. Song, Y. Yan, R. Zhang, D. Xu, F. Wang, J. Mater. Process. Technol. **120**, 237 (2002)
[49] W.W. Wits, S.J. Weitkamp, J. van Es, Procedia CIRP **7**, 252 (2013)
[50] S. Hou, S. Qi, D.A. Hutt, J.R. Tyrer, M. Mu, Z. Zhou, J. Mater. Process. Technol. **254**, 310 (2018)
[51] M. Wong, I. Owen, C.J. Sutcliffe, Heat Transf. Eng. **30**, 1068 (2009)
[52] M. Zenou, O. Ermak, A. Saar, Z. Kotler, J. Phys. D. Appl. Phys. **47**, 25501 (2013)
[53] T.K.M.K. HayashiMaekawaTamuraHanyu, JSME Int. J. Ser. A Solid Mech. Mater. Eng. **48**, 369 (2005)
[54] D.A. Hollander, M. von Walter, T. Wirtz, R. Sellei, B. Schmidt-Rohlfing, O. Paar, H.J. Erli, Biomaterials **27**, 955 (2006)
[55] M. Kanazawa, M. Iwaki, S. Minakuchi, N. Nomura, J. Prosthet. Dent. **112**, 1441 (2014)
[56] D. Lin, C.R. Liu, G.J. Cheng, Acta Mater. **80**, 183–193 (2014)
[57] D. Lin, C. Ye, Y. Liao, S. Suslov, R. Liu, G.J. Cheng, J. Appl. Phys. **113**(13), 133509 (2013)
[58] D. Lin, C. Richard Liu, G.J. Cheng, J. Appl. Phys. **115**(11), 113513 (2014)
[59] Z.H. Liu, D.Q. Zhang, S.L. Sing, C.K. Chua, L.E. Loh, Mater. Charact. **94**, 116 (2014)
[60] M. Erdal, S. Dag, Y. Jande, C.M. Tekin, Materials Science Forum, *Multiscale,* in *Multifunct*. Funct. Graded Mater., (Trans Tech Publications Ltd, 2010), pp. 253-258
[61] V.E. Beal, P. Erasenthiran, C.H. Ahrens, P. Dickens, Proc. Inst. Mech. Eng. Part B J. Eng. Manuf. **221**, 945 (2007)
[62] D. Gu, Y.C. Hagedorn, W. Meiners, G. Meng, R.J.S. Batista, K. Wissenbach, R. Poprawe, Acta Mater. **60**, 3849 (2012)
[63] R. Larson, U.S. Patent 5,786,562, July 1998
[64] W.J. Sames, F.A. List, S. Pannala, R.R. Dehoff, S.S. Babu, Int. Mater. Rev. **61**, 315 (2016)
[65] L.E. Murr, S.M. Gaytan, D.A. Ramirez, E. Martinez, J. Hernandez, K.N. Amato, P.W. Shindo, F.R. Medina, R.B. Wicker, J. Mater. Sci. Technol. **28**, 1 (2012)
[66] L. Loeber, S. Biamino, U. Ackelid, S. Sabbadini, P. Epicoco, P. Fino, J. Eckert, in, *Solid Freeform Fabrication Symposium* (Conference paper of 22nd International symposium Solid freeform fabrication proceedings, University of Texas, Texas, Austin, 2011), pp. 547–556
[67] J. Karlsson, A. Snis, H. Engqvist, J. Lausmaa, J. Mater. Process. Technol. **213**, 2109 (2013)
[68] J.K. Algardh, T. Horn, H. West, R. Aman, A. Snis, H. Engqvist, J. Lausmaa, O. Harrysson, Addit. Manuf. **12**, 45 (2016)
[69] V. Petrovic, R. Ninerola, Aircr. Eng. Aerosp. Technol. Int. J. **87**, 147 (2015)
[70] A. Saboori, A. Abdi, S.A. Fatemi, G. Marchese, S. Biamino, H. Mirzadeh, Mater. Sci. Eng. A **792**, 139822 (2020)
[71] H.P. Tang, M. Qian, N. Liu, X.Z. Zhang, G.Y. Yang, J. Wang, JOM **67**, 555 (2015)
[72] G. Del Guercio, M. Galati, A. Saboori, P. Fino, L. Iuliano, Acta Metall. Sin. Engl. Lett. **33**, 183 (2020)
[73] J. Wang, H. Tang, Mater. Technol. **31**, 86 (2016)
[74] L.E. Murr, S.M. Gaytan, A. Ceylan, E. Martinez, J.L. Martinez, D.H. Hernandez, B.I. Machado, D.A. Ramirez, F. Medina, S. Collins, R.B. Wicker, Acta Mater. **58**, 1887 (2010)
[75] S. Biamino, A. Penna, U. Ackelid, S. Sabbadini, O. Tassa, P. Fino, M. Pavese, P. Gennaro, C. Badini, Intermetallics **19**, 776 (2011)
[76] H.P. Tang, G.Y. Yang, W.P. Jia, W.W. He, S.L. Lu, M. Qian, Mater. Sci. Eng. A **636**, 103 (2015)
[77] J. Schwerdtfeger, C. Körner, Intermetallics **49**, 29 (2014)
[78] P. Drescher, H. Seitz, RTeJournal-Fachforum Fur Rapid Technol. **2015**, 1 (2015)
[79] A. L. A. Koptyug, L.E. Rännar, M. Bäckström, in, *Proceedings of the International Conference on Additive Manufacturing and 3D Printing* (Nottingham, 2013)
[80] G. Del Guercio, M. Galati, A. Saboori, Met. Mater. Int. **27**, 55 (2021)
[81] L.E. Rännar, A. Koptyug, J. Olsén, K. Saeidi, Z. Shen, Addit. Manuf. **17**, 106 (2017)
[82] Y. Zhong, L.E. Rännar, S. Wikman, A. Koptyug, L. Liu, D. Cui, Z. Shen, Fusion Eng. Des. **116**, 24 (2017)
[83] R.R. Dehoff, M.M. Kirka, W.J. Sames, H. Bilheux, A.S. Tremsin, L.E. Lowe, S.S. Babu, Mater. Sci. Technol. **31**, 931 (2015)
[84] S.P. Narra, R. Cunningham, J. Beuth, A.D. Rollett, Addit. Manuf. **19**, 160 (2018)
[85] T.T. Roehling, S.S.Q. Wu, S.A. Khairallah, J.D. Roehling, S.S. Soezeri, M.F. Crumb, M.J. Matthews, Acta Mater. **128**, 197 (2017)
[86] D.S. Shim, G.Y. Baek, J.S. Seo, G.Y. Shin, K.P. Kim, K.Y. Lee, Opt. Laser Technol. **86**, 69 (2016)
[87] F. Mazzucato, S. Tusacciu, M. Lai, S. Biamino, M. Lombardi, A. Valente, Technologies **5**, 29 (2017)
[88] S.B. Gibson I, Rosen D, Directed Energy Deposition Processes., in Additive Manufacturing Technologies: 3D Printing, Rapid Prototyping, and Direct Digital Manufacturing. ed. by I. Gibson, D. Rosen, B. Strucker (Springer-Verlag New York, 2015), pp. 245-268
[89] W.E. Frazier, J. Mater. Eng. Perform. **23**, 1917 (2014)
[90] T.D. Ngo, A. Kashani, G. Imbalzano, K.T.Q. Nguyen, D. Hui, Compos. Part B Eng. **143**, 172 (2018)
[91] C. Selcuk, Powder Met. **54**, 94 (2011)
[92] X. Wang, M. Jiang, Z. Zhou, J. Gou, D. Hui, Compos. Part B Eng. **110**, 442 (2017)
[93] M. Ma, Z. Wang, X. Zeng, Mater. Charact. **106**, 420 (2015)
[94] S.H. Riza, S.H. Masood, C. Wen, D. Ruan, S. Xu, Mater. Des. **64**, 650 (2014)
[95] S.R. Bhavar. V. Kattire, P. Patil, S. Khot, K. Gujar, in, *4th International conference and exhibition on additive manufacturing technologies* (2014)
[96] S.A. Khairallah, A.T. Anderson, A. Rubenchik, W.E. King, Acta Mater. **108**, 36 (2016)
[97] T.M. Mower, M.J. Long, Mater. Sci. Eng. A **651**, 198 (2016)
[98] A. Saboori, S. Biamino, S. Tusacciu, E. Reggio, M. Busatto, M. Lai, P. Fino, M. Lombardi, in, *Euro PM2017 Congress and Exhibition* (2017), pp. 1–5
[99] A. Saboori, G. Piscopo, M. Lai, A. Salmi, S. Biamino, Mater. Sci. Eng. A **780**, 139179 (2020)
[100] M. Aristizabal, P. Jamshidi, A. Saboori, S.C. Cox, M.M. Attallah, Mater. Lett. **259**, 126897 (2020)
[101] B. Jiang, L. Zhenglong, C. Xi, L. Peng, L. Nannan, C. Yanbin, Ceram. Int. **45**, 5680 (2019)
[102] J.H. Martin, B.D. Yahata, J.M. Hundley, J.A. Mayer, T.A. Schaedler, T.M. Pollock, Nature **549**, 365 (2017)

[103] X.P. Li, G. Ji, Z. Chen, A. Addad, Y. Wu, H.W. Wang, J. Vleugels, J. Van Humbeeck, J.P. Kruth, Acta Mater. **129**, 183 (2017)
[104] A. Saboori, M. Pavese, C. Badini, P. Fino, Front. Mater. Sci. **11**, 171 (2017)
[105] A. Saboori, X. Chen, C. Badini, P. Fino, M. Pavese, Trans. Nonferrous Met. Soc. China **29**, 657 (2019)
[106] J.M. Torralba, C.E. da Costa, F. Velasco, J. Mater. Process. Technol. **133**, 203 (2003)
[107] B. Chen, X. Xi, C. Tan, X. Song, Curr. Opin. Chem. Eng. **28**, 28 (2020)
[108] J. Wu, X.Q. Wang, W. Wang, M.M. Attallah, M.H. Loretto, Acta Mater. **117**, 311 (2016)
[109] D. Gu, Y. Yang, L. Xi, J. Yang, M. Xia, Opt. Laser Technol. **119**, 105600 (2019)
[110] K.G. Prashanth, J. Eckert, J. Alloys Compd. **707**, 27 (2017)
[111] D. Gu, X. Rao, D. Dai, C. Ma, L. Xi, K. Lin, Addit. Manuf. **29**, 100801 (2019)
[112] Z. Lei, J. Bi, Y. Chen, X. Chen, X. Qin, Z. Tian, Powder Technol. **356**, 594 (2019)
[113] J. Jue, D. Gu, J. Compos. Mater. **51**, 519 (2017)
[114] S. Lathabai, Additive Manufacturing of Aluminium-Based Alloys and Composites, in *Fundamentals of Aluminium Metallurgy*. ed. by R.N. Lumley (Woodhead Publishing, Sawston, 2018), pp. 47–92
[115] X. Wen, Q. Wang, Q. Mu, N. Kang, S. Sui, H. Yang, X. Lin, W. Huang, Mater. Sci. Eng. A **745**, 319 (2019)
[116] F. Rikhtegar, S.G. Shabestari, H. Saghafian, J. Alloys Compd. **723**, 633 (2017)
[117] W. Zhou, M. Dong, Z. Zhou, X. Sun, K. Kikuchi, N. Nomura, A. Kawasaki, Carbon **141**, 67 (2019)
[118] Y. Ma, G. Ji, X.P. Li, C.Y. Chen, Z.Q. Tan, A. Addad, Z.Q. Li, T.B. Sercombe, J.P. Kruth, Materialia **5**, 100242 (2019)
[119] J.K. Tiwari, A. Mandal, N. Sathish, A.K. Agrawal, A.K. Srivastava, Addit. Manuf. **33**, 101095 (2020)
[120] Z. Hu, F. Chen, J. Xu, Q. Nian, D. Lin, C. Chen, X. Zhu, Y. Chen, M. Zhang, J. Alloys Compd. **746**, 269 (2018)
[121] P. Bai, Y. Jin, Z. Zhao, L. Li, M. Liang, H. Liao, W. Zhao, Y. Hu, W. Du, Mater. Res. Express **6**, 1065cl (2019)
[122] J.C. Li, X. Lin, N. Kang, J.L. Lu, Q.Z. Wang, W.D. Huang, J. Alloys Compd. **826**, 154077 (2020)
[123] C. Gao, Z. Wang, Z. Xiao, D. You, K. Wong, A.H. Akbarzadeh, J. Mater. Process. Technol. **281**, 116618 (2020)
[124] H. Tan, D. Hao, K. Al-Hamdani, F. Zhang, Z. Xu, A.T. Clare, Mater. Lett. **214**, 123 (2018)
[125] X. Zhao, D. Gu, C. Ma, L. Xi, H. Zhang, Vacuum **160**, 189 (2019)
[126] L. Wu, Z. Zhao, P. Bai, W. Zhao, Y. Li, M. Liang, H. Liao, P. Huo, J. Li, Appl. Surf. Sci. **503**, 144156 (2020)
[127] C. Gao, Z. Liu, Z. Xiao, W. Zhang, K. Wong, A.H. Akbarzadeh, J. Alloys Compd. **853**, 156722 (2020)
[128] F. Chang, D. Gu, D. Dai, P. Yuan, Surf. Coat. Technol. **272**, 15 (2015)
[129] P. Wang, C. Gammer, F. Brenne, T. Niendorf, J. Eckert, S. Scudino, Compos. Part B Eng. **147**, 162 (2018)
[130] A. Saboori, S. Biamino, M. Lombardi, S. Tusacciu, M. Busatto, M. Lai, P. Fino, Powder Metall. **62**, 213 (2019)
[131] L. Yan, X. Chen, W. Li, J. Newkirk, F. Liou, J. Newkirk, F. Liou, J. Alloy. Compd. **22**, 810 (2016)
[132] I.V. Okulov, A.S. Volegov, H. Attar, M. Bönisch, S. Ehtemam-Haghighi, M. Calin, J. Eckert, J. Mech. Behav. Biomed. Mater. **65**, 866 (2017)
[133] K. Kondoh, 16-Titanium Metal matrix composites by powder metallurgy (PM) routes, in *Titanium Powder Metallurgy*, ed. by M. Qian and F. H. (Sam) Froes (Butterworth-Heinemann, Boston, 2015), pp. 277–297
[134] Y. Liu, L.F. Chen, H.P. Tang, C.T. Liu, B. Liu, B.Y. Huang, Mater. Sci. Eng. A **418**, 25 (2006)
[135] A. Saboori, S. Tusacciu, M. Busatto, M. Lai, S. Biamino, P. Fino, M. Lombardi, J. Vis. Exp. **2018**, e56966 (2018)
[136] B. Baufeld, O. Van der Biest, R. Gault, Mater. Des. **31**, S106 (2010)
[137] H. Attar, S. Ehtemam-Haghighi, D. Kent, M.S. Dargusch, Int. J. Mach. Tools Manuf. **133**, 85 (2018)
[138] J. Wang, L. Li, C. Tan, H. Liu, P. Lin, J. Mater. Process. Technol. **252**, 524 (2018)
[139] S. Liu, Y.C. Shin, Mater. Des. **136**, 185 (2017)
[140] S. M. Artem Builuk, Marina Kazachenok, in *AIP Conference Proceedings 2167, 020039* (2019)
[141] L. Li, J. Wang, P. Lin, H. Liu, Ceram. Int. **43**, 16638 (2017)
[142] C.A. Terrazas, L.E. Murr, D. Bermudez, E. Arrieta, D.A. Roberson, R.B. Wicker, J. Mater. Sci. Technol. **35**, 309 (2019)
[143] Y. Liu, S. Li, R.D.K. Misra, K. Geng, Y. Yang, Scr. Mater. **183**, 6 (2020)
[144] P.K. Farayibi, T.E. Abioye, A. Kennedy, A.T. Clare, J. Manuf. Process. **45**, 429 (2019)
[145] H. Li, Z. Yang, D. Cai, D. Jia, Y. Zhou, Mater. Des. **185**, 108245 (2020)
[146] H. Attar, M. Bönisch, M. Calin, L.C. Zhang, S. Scudino, J. Eckert, Acta Mater. **76**, 13 (2014)
[147] B. He, K. Chang, W. Wu, C. Zhang, Vacuum **143**, 23 (2017)
[148] Y. Hu, W. Cong, X. Wang, Y. Li, F. Ning, H. Wang, Compos. Part B Eng. **133**, 91 (2018)
[149] H. Attar, S. Ehtemam-Haghighi, D. Kent, I.V. Okulov, H. Wendrock, M. Bönisch, A.S. Volegov, M. Calin, J. Eckert, M.S. Dargusch, Mater. Sci. Eng. A **688**, 20 (2017)
[150] J. Jin, S. Zhou, Y. Zhao, Q. Zhang, X. Wang, W. Li, D. Chen, L.C. Zhang, Opt. Laser Technol. **134**, 106644 (2021)
[151] D. Gu, Y.C. Hagedorn, W. Meiners, K. Wissenbach, R. Poprawe, Surf. Coatings Technol. **205**, 3285 (2011)
[152] P. Krakhmalev, I. Yadroitsev, Intermetallics **46**, 147 (2014)
[153] G. Chen, R.Z. Liu, Y.D. Qiu, Y. Yang, J.M. Wu, S.F. Wen, J. Liu, Y.S. Shi, H.B. Tan, Mater. Today Commun. **24**, 101114 (2020)
[154] M. Das, V.K. Balla, D. Basu, S. Bose, A. Bandyopadhyay, Scr. Mater. **63**, 438 (2010)
[155] K. Morsi, V.V. Patel, J. Mater. Sci. **42**, 2037 (2007)
[156] Y. Horiuchi, T. Inamura, H.Y. Kim, K. Wakashima, S. Miyazaki, H. Hosoda, Mater. Trans. **48**, 407 (2007)
[157] H. Attar, M. Bönisch, M. Calin, L.C. Zhang, K. Zhuravleva, A. Funk, S. Scudino, C. Yang, J. Eckert, J. Mater. Res. **29**, 1941 (2014)
[158] M. Xia, A. Liu, Z. Hou, N. Li, Z. Chen, H. Ding, J. Alloys Compd. **728**, 436 (2017)
[159] C.L. Wu, S. Zhang, C.H. Zhang, J.B. Zhang, Y. Liu, J. Chen, Opt. Laser Technol. **115**, 134 (2019)
[160] B. AlMangour, Y.K. Kim, D. Grzesiak, K.A. Lee, Compos. Part B Eng. **156**, 51 (2019)
[161] X. Li, C.H. Zhang, S. Zhang, C.L. Wu, J.B. Zhang, H.T. Chen, A.O. Abdullah, Vacuum **165**, 139 (2019)
[162] D. Tanprayoon, S. Srisawadi, Y. Sato, M. Tsukamoto, T. Suga, Opt. Laser Technol. **129**, 106238 (2020)
[163] G. Lian, C. Zhao, Y. Zhang, X. Huang, C. Chen, J. Jiang, Coatings **9**, 498 (2019)
[164] D.E. Cooper, N. Blundell, S. Maggs, G.J. Gibbons, J. Mater. Process. Technol. **213**, 2191 (2013)
[165] L. Chen, Y. Sun, L. Li, X. Ren, Corros. Sci. **169**, 108606 (2020)
[166] Y. Wang, J. Shi, J. Manuf. Sci. Eng. **142**, 5 (2020)
[167] L. Constantin, L. Fan, M. Pontoreau, F. Wang, B. Cui, J.L. Battaglia, J.F. Silvain, Y.F. Lu, Manuf. Lett. **24**, 61 (2020)
[168] Y.C. Zhao, Y. Tang, M.C. Zhao, C. Liu, L. Liu, C.D. Gao, C. Shuai, A. Atrens, JOM **72**, 1163 (2020)
[169] S.J. Hollister, Nat. Mater. **4**, 518 (2005)